Analytical and numerical analysis of tides and salinities in estuaries; part I: tidal wave propagation in convergent estuaries

Leo C. van Rijn

Ocean Dynamics
Theoretical, Computational and Observational Oceanography

ISSN 1616-7341
Volume 61
Number 11

Ocean Dynamics (2011) 61:1719-1741
DOI 10.1007/s10236-011-0453-0

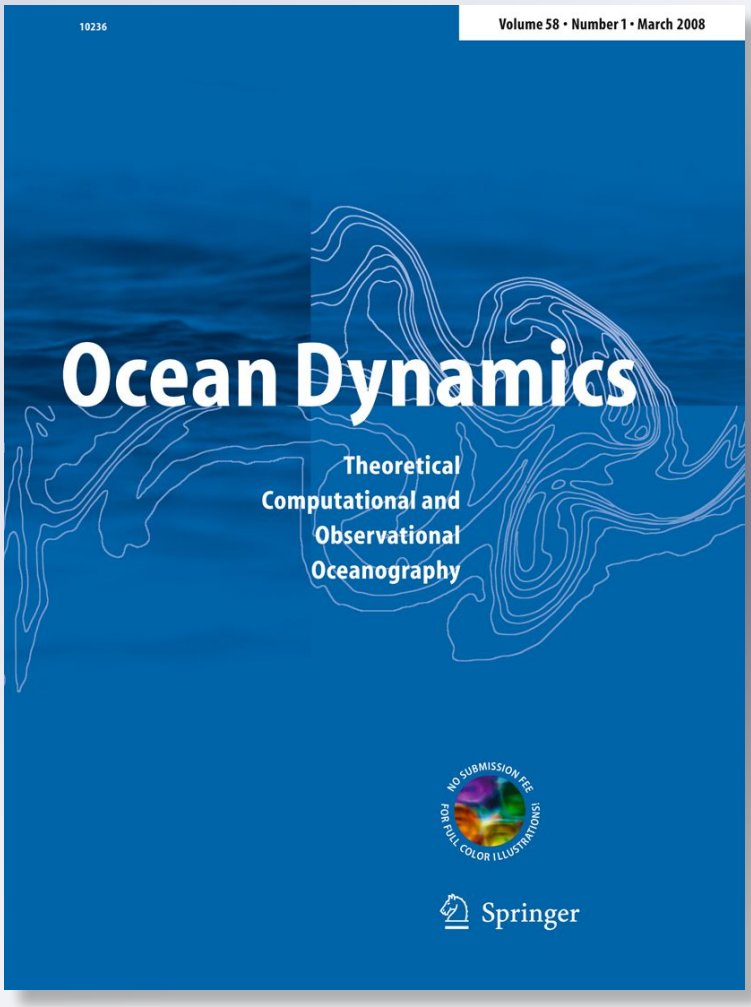

Springer

Your article is protected by copyright and all rights are held exclusively by Springer-Verlag. This e-offprint is for personal use only and shall not be self-archived in electronic repositories. If you wish to self-archive your work, please use the accepted author's version for posting to your own website or your institution's repository. You may further deposit the accepted author's version on a funder's repository at a funder's request, provided it is not made publicly available until 12 months after publication.

Springer

Author's personal copy

Ocean Dynamics (2011) 61:1719–1741
DOI 10.1007/s10236-011-0453-0

Analytical and numerical analysis of tides and salinities in estuaries; part I: tidal wave propagation in convergent estuaries

Leo C. van Rijn

Received: 3 February 2011 / Accepted: 9 June 2011 / Published online: 10 July 2011
© Springer-Verlag 2011

Abstract Analytical solutions of the momentum and energy equations for tidal flow are studied. Analytical solutions are well known for prismatic channels but are less well known for converging channels. As most estuaries have a planform with converging channels, the attention in this paper is fully focused on converging tidal channels. It will be shown that the tidal range along converging channels can be described by relatively simple expressions solving the energy and momentum equations (new approaches). The semi-analytical solution of the energy equation includes quadratic (nonlinear) bottom friction. The analytical solution of the continuity and momentum equations is only possible for linearized bottom friction. The linearized analytical solution is presented for sinusoidal tidal waves with and without reflection in strongly convergent (funnel type) channels. Using these approaches, simple and powerful tools (spreadsheet models) for tidal analysis of amplified and damped tidal wave propagation in converging estuaries have been developed. The analytical solutions are compared with the results of numerical solutions and with measured data of the Western Scheldt Estuary in the Netherlands, the Hooghly Estuary in India and the Delaware Estuary in the USA. The analytical solutions show surprisingly good agreement with measured tidal ranges in these large-scale tidal systems. Convergence is found to be dominant in long and deep-converging channels resulting in an amplified tidal range, whereas bottom friction is generally dominant in shallow converging channels resulting in a damped tidal range. Reflection in closed-end channels is important in the most landward 1/3 length of the total channel length. In strongly convergent channels with a single forward propagating tidal wave, there is a phase lead of the horizontal and vertical tide close to 90°, mimicking a standing wave system (apparent standing wave).

Keywords Tidal propagation · Salinity · Convergent estuary · Prismatic channel · Analytical model · Numerical model

Responsible Editor: Roger Proctor

L. C. van Rijn (✉)
Deltares and University of Utrecht,
Utrecht, The Netherlands
e-mail: leo.vanrijn@deltares.nl

1 Introduction

The shape of most alluvial estuaries is similar all over the world, see Dyer (1997), McDowell and O'Connor (1977), Savenije (2005), and Prandle (2009). The width and the area of the cross-section reduce in upstream (landward) direction with a river outlet at the end of the estuary resulting in a converging (funnel shape) channel system (see Fig. 1). The bottom of the tide-dominated section generally is fairly horizontal. Often, there is a mouth bar at the entrance of the estuary. Tidal flats or islands may be present along the estuary (deltas).

The tidal range in estuaries is affected by four dominant processes: (a) inertia related to acceleration an deceleration effects, (b) amplification (or shoaling) due to the decrease of the width and depth (convergence) in landward direction and (c) damping due to bottom friction, and (d) partial reflection at landward end of the estuary, whereas bathymetric convergence produces continuous reflection along the entire length of the channel (see point b).

The classical solution of the linearized mass and momentum balance equations for a *prismatic* channel of constant depth and width is well-known (Hunt 1964;

Author's personal copy

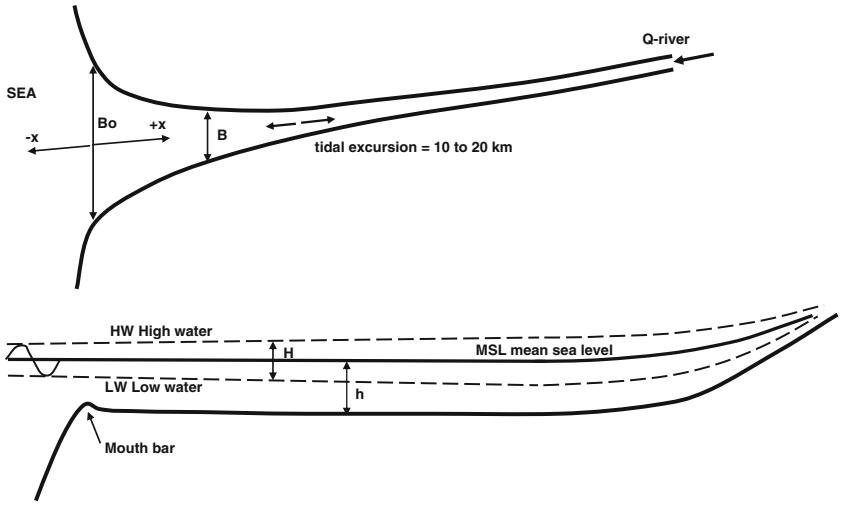

Fig. 1 Tidal estuary (planform and longitudinal section)

Dronkers 1964, 2005; Ippen 1966; Le Blond 1978; Verspuy 1985; Prandle 2009). This solution for a prismatic channel represents an exponentially damped sinusoidal wave which dies out gradually in a channel with an open end or is reflected in a channel with a closed landward end. In a frictionless system with depth h_o, both the incoming and reflected wave have a phase speed of $c_o=(gh_o)^{0.5}$ and have equal amplitudes resulting in a standing wave with a virtual wave speed equal to infinity due to superposition of the incoming and reflected wave. Including (linear) friction, the wave speed of each wave is smaller than the classical value c_o (damped co-oscillation). According to Le Blond (1978), frictional forces dominate accelerations over most of the tidal cycle and hence a diffusive type of solution (neglecting accelerations) provides accurate results for most of the tydal cycle in a prismatic channel. Using the classical approach, the tidal wave propagation in a funnel-type estuary can only be considered by schematizing the channel into a series of prismatic subsections, each with its own constant width and depth, following Dronkers (1964) and many others. Unfortunately, this approach eliminates to a large extent the effects of convergence in width and depth on the complex wave number and thus on the wave speed (Jay 1991). A better approach is to represent the planform of the estuary by a geometric function. When an exponential function with a single-length scale parameter (L_b) is used, the linearized equations can still be solved analytically and are of an elegant simplicity.

The analytical solution for a funnel-type channel with exponential width and constant depth is, however, not very well known. Hunt was one of the first to explore analytical solutions for converging channels using exponential and power functies to represent the width variations. Both Le Floch (1961) and Hunt (1964) have given solutions for exponentially converging channels with constant depth. However, their equations are not very transparent. Furthermore, they have not given the full solution including the precise damping coefficient and wave speed expressions for both amplified and damped converging channels. Hunt (1964) briefly presents his solution for a converging channel and focusses on an application for the Thames Estuary in England. The analytical model is found to give very reasonable results fitting the friction coefficient. Hunt shows that strongly convergent channels can produce a single forward-propagating tidal wave with a phase lead of the horizontal and vertical tide close to 90°, mimicking a standing wave system (apparent standing wave). A basic feature of this system is that the wave speed is much larger than the classical value $c_o=(gh_o)^{0.5}$, in line with observations. For example, the observed speed of the tidal wave in the amplified Western Scheldt Estuary in The Netherlands is between 11 and 15 m/s, whereas the classical value is of about 10 m/s.

Parker (1984) has given a particular solution for a converging tidal channel with a closed-end focusing on the tidal characteristics (only sinusoidal (M_2) tide) of the Delaware Estuary (USA). He shows that the solution based on linear friction and exponential decreasing width yields very reasonable results for the Delaware Estuary fitting the friction coefficient.

Harleman (1966) also included the effect of width convergence by combining Greens' law and the expressions for a prismatic channel. Predictive expressions for the friction coefficient and wave speed were not given. Instead, he used measured tidal data to determine the friction coefficient and wave length.

Godin (1988) and Prandle and Rahman (1980) have addressed a channel with both converging width and depth. They show that that the analytical solution can be formulated in terms of Bessel functions for tidal elevations and tidal velocities in open and closed channels. However, the complex Bessel functions involved obscure any

Author's personal copy

immediate physical interpretation. Therefore, their results were illustrated in diagrammatic form (contours of amplitude and phase) for a high- and low-friction coefficient.

Like Hunt, Jay (1991), based on an analytical perturbation model of the momentum equation for convergent channels (including river flow and tidal flats), has shown that a single, incident tidal wave may mimic a standing wave by having an approximately 90° phase difference between the tidal velocities and tidal surface elevations and a very large wave speed without the presence of a reflected wave. The tidal wave behavior to lowest order is dominated by friction and the rate channel convergence. This result is confirmed by the energy-based approach presented herein. Friedrichs and Aubrey (1994) have presented a first-order solution of tidal wave propagation which retains and clarifies the most important properties of tides in strongly convergent channels with both weak and strong friction. Their scaling analysis of the continuity and momentum equation clearly shows that the dominant effects are: friction, surface slope, and along-channel gradients of the cross-sectional area (rate of convergence). Local advective acceleration is much smaller than the other contributions.

Lanzoni and Seminara (1998) have presented linear and nonlinear solutions for tidal propagation in weakly and strongly convergent channels by considering four limiting cases defined by the relative strength of dissipation versus local inertia and convergence. In weakly dissipative channels, the tidal propagation is essentially a weakly nonlinear problem. As channel convergence increases, the distortion of the tidal wave is enhanced and both the tidal wave speed and height increase leading to ebb dominance. In strongly dissipative channels, the tidal wave propagation is a strongly nonlinear process with strong distortion of the wave profile leading to flood dominance. They use a nonlinear parabolic approximation of the full momentum equation.

Prandle (2003a, b) has presented localized analytical solutions for the propagation of a single tidal wave in channels with strongly convergent *triangular* cross-sections, neglecting the advective terms and linearizing the friction term. The solutions apply at any location where the cross-sectional shape remains reasonably congruent and the spatial gradient of tidal elevation amplitude is relatively small (ideal or synchronous estuary). Analyzing the tidal characteristics of some 50 estuaries, he proposed an expression for the bed friction coefficient as function of the mud content yielding a decreasing friction coefficient for increasing mud content.

Finally, Savenije et al. (2008) have presented analytical solutions of the 1D hydrodynamic equations in a set of four equations for the tidal amplitude, the peak tidal velocity, the wave speed, and the phase difference between horizontal and vertical tide. Only bulk parameters are considered; hence, the time effect is not resolved. Since reflection is not considered, their equations cannot deal with closed-end channels. Various approaches have been used to arrive at their four equations. According to the authors, the combination of different approaches may introduce inconsistencies, which may limit the applicability of the equations. This may not be a real problem as long as measured data sets are available for calibration of the tidal parameters.

In this paper, analytical solutions of the momentum and energy equations for converging tidal channels are presented. The basic tidal equations are presented in Section 2. After that in Section 3, an energy-based approach is introduced for converging tidal channels including quadratic (nonlinear) bottom friction. It will be shown that the tidal range (H) can be simply related to the friction parameter and the rate of channel convergence. Then, an analytical solution of the linearized equations of continuity and momentum for converging tidal channels will be presented (Section 4). The linearized analytical solution of the equations of continuity and momentum is presented for M_2 tidal waves with and without reflection in strongly convergent (funnel type) channels. This latter analytical solution involves three cases: case A=synchronous tidal channel with constant tidal range, case B=amplified tidal range, and case C=damped tidal range. Focusing on semidiurnal M_2 tides, the present approach applies to midlatitude estuaries.

Both approaches (energy and momentum equations) offer simple and powerful tools (spreadsheet models) for tidal analysis of amplified and damped tidal wave propagation in converging estuaries. The analytical solutions are compared with the results (Section 5) of measured data of the Western Scheldt Estuary in the Netherlands, the Hooghly Estuary in India, and the Delaware Estuary in the USA. The analytical solutions of the energy flux equation and the linearized continuity–momentum equations show surprisingly good agreement with measured tidal ranges in these large-scale tidal systems. Section 6 presents comparison results of the analytical and numerical models.

It is noted that the linearized solution cannot deal with the various sources of nonlinearity such as quadratic friction, finite amplitude, variation of the water depth under the crest and trough, effects of river flow, and effects of tidal flats causing differences in wave speed and hence wave deformation (see Jay 1991). In Section 7, these effects are discussed for a series of schematized cases based on detailed numerical solutions including all terms. One-dimensional numerical models can be setup easily and quickly and produce fairly accurate results if the geometry and topography is resolved in sufficient detail. Analytical

Author's personal copy

models can only deal with schematized cases, but offer the advantage of simplicity and transparency. Simple spreadsheet solutions can be made for a quick scan of the parameters involved. The usefulness of the present analytical approaches is that the effects of human interventions such as channel deepening and widening can be assessed quickly (quick scans). The simple analytical tidal models can be easily combined with salt intrusion models (see part II), sediment transport models, ecological models, etc. for a quick first analysis of the problems involved. Based on this, the parameter range can be narrowed down substantially so that the minimum number of detailed numerical model runs need to be made.

2 Basic equations of continuity and momentum

A clear understanding of the relative importance of the terms of the equations of continuity and momentum can be obtained by scaling analysis. Based on measured data from three very different tidal systems with depths in the range of 5–10 m and decreasing widths and cross-sectional areas, Friedrichs (1993) and Friedrichs and Aubrey (1994) have convincingly shown that the e-folding length scale L_b of the width (width $b=b_o \exp(-x/L_b)$) and the e-folding length scale L_A of the cross-sectional area (cross-sectional area $A=A_o \exp(-x/L_A)$) are of the same order of magnitude and are much smaller than the length scale L_U of the horizontal velocity variations. This implies that the nonlinear convective acceleration term ($\overline{\overline{u}}\partial\overline{\overline{u}}/\partial x$; $\overline{\overline{u}}$ = cross-section-averaged velocity) is negligibly small in the major part of the estuary with exception of the region close to the landward boundary where a river (open end) or a zero tidal flow boundary (closed end) may be present. In most estuaries with a loose sediment bed, the peak horizontal velocity is almost constant (of the order of 1 m/s) along the channel due to morphological adjustment, which causes the tidal velocity to be rather uniform in space. If horizontal velocity gradients will exist, then the channels will not be stable resulting in net deposition in regions of relatively low bed–shear stresses and net erosion in regions with relatively high bed–shear stresses. For the channels considered by Friedrichs and Aubrey (1994), the along-channel gradients in discharge are dominated by along-channel gradients in cross-sectional area as regards the continuity equation. They also show that the local acceleration term $\left(\partial\overline{\overline{u}}/\partial t\right)$ is relatively small compared to the other terms. The two most important terms of the momentum equation are the pressure term (water surface slope term) and the frictional term.

Neglecting the convective acceleration term ($\overline{\overline{u}}\partial\overline{\overline{u}}/\partial x$, very small in tidal channels; see Friedrichs and Aubrey 1994, Jay 1991, and Van Rijn 1993, 2011), the equations of continuity and motion for depth-averaged flow in a channel with a rectangular cross-section are:

$$\frac{b\partial\eta}{\partial t}+\frac{\partial Q}{\partial x}=0 \tag{1}$$

$$\frac{1}{A}\frac{\partial Q}{\partial t}+\frac{g}{}\frac{\partial\eta}{\partial x}+\frac{Q|Q|}{C^2A^2R}=0 \tag{2}$$

in which, $A=bh_o$=area of cross-section, b=surface width, h_o=depth to mean sea level (MSL), R=hydraulic radius ($\cong h_o$ if $b \gg h_o$), η=water level to mean sea level, Q=discharge=$A\overline{\overline{u}}$, $\overline{\overline{u}}$=cross-section-averaged velocity, and C=Chézy coefficient (constant).

Similar equations can be derived for compound channels (Van Rijn 2011).

3 Energy-based approach

The principle of tidal wave amplification defined as the increase of the wave height due to the gradual change of the geometry of the system (depth and width) can be easily understood by considering the wave energy flux equation, which is known as Green's law (1837). This phenomenon is also known as wave shoaling or wave funneling. The total energy of a sinusoidal tidal wave per unit length is equal to $E=0.125\ \rho g\ bH^2$ with b=width of channel and H=wave height. The propagation velocity of a sinusoidal wave is given by $c_o=(gh_o)^{0.5}$ with h_o=water depth.

Assuming that there is no reflection and no loss of energy (due to bottom friction), the energy flux (see Eq. 3) is constant resulting in: $E_o c_o = E_x c_x$ or $H_x/H_o = (b_x/b_o)^{-0.5}(h_x/h_o)^{-0.25}$. Thus, the tidal wave height H_x increases for decreasing width and depth. The wave length $L=c_o T$ will decrease as c_o will decrease for decreasing depth resulting in a shorter and higher wave.

The variation of the tidal range H in a real estuary with exponentially decreasing width and depth can be derived from an overall energy-based approach including bottom friction. The width and depth are assumed to vary exponentially.

Waves transfer energy in horizontal direction during wave propagation. To be able to propagate itself, a wave must transfer energy to the fluid in rest in front of the wave. The rate at which energy is transferred from one section to another section is known as energy flux F. Basically, it is the time-averaged work done by the dynamic pressure force per unit time during a wave period, like in short-wave theory. Wave energy is extracted from the system through the work done by the bed shear stress (causing wave damping). It is realized that the representation of a tidal wave by a single progressive sinusoidal wave is a crude schematization of a real distorted tidal wave (including

Author's personal copy

reflection) in an estuary. Therefore, this method only yields a first-order description of the bulk parameters involved (tidal range H) for conditions without much reflection.

The energy flux balance for depth-integrated tidal flow reads, as:

$$d(\mathrm{b}\overline{F})/dx + b\,D_w = 0 \tag{3}$$

$$b\ \mathrm{d}\overline{F}/\mathrm{dx} + \overline{F}\mathrm{db}/\mathrm{dx} + b\ D_w = 0 \tag{4}$$

with $\overline{F}$=energy flux per unit width per unit time and D_w= energy dissipation per unit area and time due to bottom friction, b=width of estuary channel, x=horizontal coordinate (positive in landward direction, x=0=mouth). The unit of each term is kilogram per m per cubic second (kg m/s^3).

The energy flux can be expressed as (see Appendix I): $\overline{F} = 0.125\,\rho g\,H^2 c_\mathrm{o} = \overline{\mathrm{E}}\mathrm{c}_\mathrm{o}$ with: $\overline{E} = 0.125\,\rho g\,H^2$=energy of a wave per unit area, c_o=wave propagation velocity. Thus, the energy flux per unit width of a progressive wave in deep water is equal to the energy of a wave per unit length of the wave and the wave propagation velocity (similar to the expression used in short wave theory).

The instantaneous energy dissipation per unit area and time due to work done by the bed–shear stresses can be expressed (see Appendix I): $\overline{D}_w = 4/(3\pi)\rho(g/C^2)\,\widehat{\overline{u}}^3$

The width and depth of the estuary channel is represented as:

$$\begin{aligned} b &= b_\mathrm{o}\exp(-\beta x) = b_\mathrm{o}\exp(-x/L_b) \text{ and thus} \\ \mathrm{db}/\mathrm{dx} &= -\beta\,\mathrm{b}_\mathrm{o}\exp(-\beta\,\mathrm{x}) = -\beta\ \mathrm{b} \\ \mathrm{h} &= \mathrm{h}_\mathrm{o}\exp(-\gamma\,\mathrm{x}) = \mathrm{h}_\mathrm{o}\exp(-\mathrm{x}/\mathrm{L}_\mathrm{h}) \text{ and thus} \\ \mathrm{dh}/\mathrm{dx} &= -\gamma\,\mathrm{h}_\mathrm{o}\exp(-\gamma\,\mathrm{x}) = -\gamma\ \mathrm{h} \end{aligned}$$

with, b_o=width at entrance x=0, β=1/L_b=width convergence coefficient, γ=1/L_h=depth convergence coefficient, L_b= convergence length scale for width, L_h=convergence length scale for depth. The length scale L_b is of the order of 10–50 km for most estuaries. The length scale L_h is much larger than L_b for most estuaries as the depth generally is fairly constant or very weakly decreasing in landward direction.

Using these expressions (see Appendix I), the solution of Eq. 4 yields:

$$\mathrm{dH}/\mathrm{dx} = 0.5(\beta+\gamma)H - \frac{f\,\widehat{\overline{u}}^2}{3\pi g\ h\ \cos\varphi} \tag{5}$$

or as γ=0:

$$\mathrm{dH}/\mathrm{dx} = 0.5\,\beta H - \frac{f\,H^2 c^2\cos\varphi}{12\pi g(h_0)^3} \tag{6}$$

with, H=tidal range, β=1/L_b=width convergence coefficient (L_b=e-folding length scale), h_o=depth (constant), $\widehat{\overline{u}}$=peak tidal velocity along channel, c=local wave speed, φ=phase difference between horizontal and vertical tide, f=8g/C^2= friction coefficient, C=Chézy coefficient, and x=horizontal coordinate (positive in landward direction).

Neglecting friction (f=0), Eq. 5 yields: dH/dx = 0.5($\beta+\gamma$) H or $H/H_\mathrm{o} = e^{0.5(\beta+\gamma)x}$. The tidal wave height increases exponentially for exponentially decreasing width and depth in line with Green's law.

Equations 5 and 6 include two terms: the effect of depth and width convergence (funneling) and the effect of quadratic (nonlinear) bottom friction. Amplification will occur if the convergence (first) term is largest. Damping will occur if the friction (second) term is largest. To produce the tidal range along the channel, it can be simply solved in a spreadsheet when $\widehat{\overline{u}}$, φ, h_o, f (or C) and the boundary condition H=H_o at x=0 are known. The $\widehat{\overline{u}}$ and φ parameters will be taken from the linearized solution of the equations of continuity and momentum (see Table 1 of Section 4) for converging channels.

In the case of a compound channel (consisting of main channel and tidal flats), the depth h_o should be replaced by the wave propagation depth $h_\mathrm{eff} = A/b_s = \alpha_h h_\mathrm{o}$ (Van Rijn 2011). Furthermore, the friction coefficient will be larger and the wave speed will be smaller in a compound channel.

Savenije (2005) has given an expression for the tidal range which is based on an analytical solution of the simplified momentum equation for a converging estuary using a Lagrangian coordinate system. The momentum equation is applied at times of high water (HW) and low water (LW) and then subtracted to determine dH/dx. His final result reads as:

$$\mathrm{dH}/\mathrm{dx}(1+\alpha) = \beta\,\mathrm{H} - f'(H/h)\left(\widehat{\overline{u}}/c\right)\cos\varphi \tag{7}$$

with c=wave speed, $\widehat{\overline{u}}$=peak tidal current velocity, φ= phase lead angle (constant), h=mean depth, β=1/L_b=width convergence coefficient, f'=g/C^2=friction coefficient and $\alpha = \mathrm{gH}/\left(2c\widehat{\overline{u}}\cos\varphi\right)$. The assumption of Savenije (2005): $\mathrm{d}\widehat{\overline{u}}/\mathrm{dx} = (\widehat{\overline{u}}/H)\ \mathrm{dH}/\mathrm{dx}$ leads to the α term, which is not present in Eq. 6. Savenije et al. (2008) have improved their method by presenting a set of four equations for the variables: H, $\widehat{\overline{u}}$, c, and φ.

Equation 6 can be used to estimate the length of a (synchronous) estuary with a constant tidal range (dH/dx=0) yielding $\beta = 1/L_b = (fH^2c^2\cos\varphi)/\left(6\pi\ g\ {h_o}^3 H\right)$.

Using c^2=$g\,h_\mathrm{o}$, it follows that the converging length scale is: $L_b = \left(6\pi {h_o}^2\right)/(f\ H\ \cos\varphi)$ for a synchronous estuary. Assuming that the length L of the synchronous part of an alluvial estuary is about $L \cong 2L_b \cong \left(12\pi\ {h_o}^2\right)/(f\ H\ \cos\varphi)$. Using f≅0.025 and cosφ≅0.7, yields that L≅2,000 (h_o/H) h_o. The ratio H/h_o is about 0.1–0.4 in the mouth of most estuaries and thus L≅(5,000–20,000)h_o. Using h_o=1–20 m, the length of funnel-shaped, synchronous, alluvial estuaries will be in the range of 5–400 km. Prandle (2004) has found

Table 1 Analytical solutions for prismatic and converging channels (with and without reflection)

Type of wave	Prismatic channels	Converging channels
Excluding reflection at landward end (channel open at end)	$\eta_{x,t} = \widehat{\eta}_o[e^{-\mu x}][\cos(\omega t - kx)]$ $\overline{\overline{u}}_{x,t} = \widehat{\overline{u}}_o[e^{-\mu x}]\cos(\omega t - kx + \varphi)$ with $\widehat{\overline{u}}_o = -(\widehat{\eta}_o/h_o)(\omega/k)[\cos\varphi]$ μ=friction parameter k=wave number φ=phase lead $\tan\varphi = \mu/k$ x=horizontal coordinate; positive in landward direction	$\eta_{x,t} = \widehat{\eta}_o[e^{-\varepsilon x}][\cos(\omega t - kx)]$ $\overline{\overline{u}}_{x,t} = \widehat{\overline{u}}_o[e^{-\varepsilon x}]\cos(\omega t - kx + \varphi)$ with $\varepsilon = -0.5\beta + \mu$ $\widehat{\overline{u}}_o = -(\widehat{\eta}_o/h_o)(\omega/k)[\cos\varphi]$ $c = \omega/k, \tan\varphi = \sin\varphi/\cos\varphi = (0.5\beta + \mu)/k,$ $\sin\varphi = (0.5\beta + \mu)/\left[(0.5\beta + \mu)^2_{0.5} + k^2\right]^{0.5}$ $\cos\varphi = (k)/\left[(0.5\beta + \mu)^2 + k^2\right]$, μ=friction parameter k=wave number φ=phase lead (between horizontal and vertical tide) $\beta = 1/L_b$=convergence parameter x=horizontal coordinate; positive in landward direction
Including reflection at landward end (channel closed at end)	$\eta_{x,t} = 0.5\overline{\eta}_o(f_A)^{-1}\left[e^{-\mu(x-L)}\cos(\omega t - k(x-L)) + e^{\mu(x-L)}\cos(\omega t + k(x-L))\right]$ $\overline{\overline{u}}_{x,t} = 0.5\omega(\widehat{\eta}_o/h_o)(f_A)^{-1}\left(k^2 + \mu^2\right)^{-0.5}$ $\left[e^{-\mu(x-L)}\cos(\omega t - k(x-L) + \varphi) - e^{\mu(x-L)}\cos(\omega t + k(x-L) + \varphi)\right]$ with f_A=amplification/damping factor= $=[\cos^2(kL)+\sinh^2(\mu L)]^{0.5}$ L=channel length x=horizontal coordinate; positive in landward direction	$\eta_{x,t} = 0.5\widehat{\eta}_o(f_A)^{-1}\left[e^{(\varepsilon 1)x+\mu L}\cos(\omega t - k(x-L)) + e^{(\varepsilon 2)x-\mu L}\cos(\omega t + k(x-L))\right]$ $\overline{\overline{u}}_{x,t} = 0.5\omega(\widehat{\eta}_o/h_o)(f_A)^{-1}(k^2 + \mu^2)^{-0.5}$ $[e^{(\varepsilon 1)x+\mu L}\cos(\omega t - k(x-L) + \varphi)]$ $-e^{(\varepsilon 2)x-\mu L}\cos(\omega t + k(x-\vec{L}) + \varphi)$ with $\varepsilon_1 = 0.5\ \beta - \mu$ $\varepsilon_2 = 0.5\beta + \mu$ f_A=amplification/damping factor= $=[\cos^2(kL)+\sinh^2(\mu L)]^{0.5}$ L=channel length, x=horizontal coordinate, positive in landward direction

Author's personal copy

Author's personal copy

$L \cong 2,500(h_o)^{1.25}/H^{0.5}$. He presents a set of 50 estuaries (UK and USA) with lengths of 2–200 km and depths of 1–20 m.

4 Analytical and numerical solutions of equations of continuity and momentum

4.1 Prismatic channels

Neglecting the convective acceleration term $\left(\overline{\overline{u}}\partial\overline{\overline{u}}/\partial x\right)$, the equations of continuity and momentum for a wide, prismatic channel with rectangular cross-section and constant mean depth $(h = h_o + \eta)$ can be linearized by replacing the quadratic friction term by a linear term (based on the Lorentz (1922, 1926) method), as follows:

$$\frac{\partial \eta}{\partial t} + \frac{h_0\,\partial\overline{\overline{u}}}{\partial x} = 0 \tag{8}$$

$$\frac{\partial\overline{\overline{u}}}{\partial t} + \frac{g\,\partial\eta}{\partial x} + m\left|\widehat{\overline{u}}\right| = 0 \tag{9}$$

in which, $\overline{\overline{u}}$=cross-section-averaged velocity, $\overline{u}$=depth-averaged velocity, $\widehat{\overline{u}}$=amplitude of close section-averaged tidal current velocity, m=friction coefficient= $\left(8g\left|\widehat{\overline{u}}\right|\right)/\left(3\pi C^2 R\right)$, R=hydraulic radius ($R \cong h_o$ and $\overline{\overline{u}} \cong \overline{u}$ for a very wide channel $b >> h_o$). Using the Lorentz method, the total linear friction over the tidal cycle is the same as that for quadratic friction. It is noted that the friction coefficient depends on the peak velocity (usually taken at x=0). The classical analytical solution of these two equations with and without reflection at the head of the channel is given in Table 1 (Dronkers 1964, 2005; Verspuy 1985; Van Rijn 1993, 2011). The solution is an exponentially damped wave due to bottom friction. The phase lead φ of the velocity with respect to the water level can be expressed as tanφ=μ/k with μ=damping coefficient, and k=wave number. The wave speed c is always smaller than the classical value $c_o=(gh_o)^{0.5}$.

The water surface slope can be expressed as: $\partial\eta/\partial x = \widehat{n}_0(e^{-\mu x})\left(\mu^2 + k^2\right)^{0.5}\cos(\omega t - kx + \psi)$ with: $\tan\psi = k/\mu$ or $\text{cotan}\psi = \mu/k$. Since $\tan\varphi = \mu/k$ (see Table 1), it follows that cotanψ=tanφ or $\psi = 90^0 - \varphi$. Thus, the velocity has a phase lag of $\psi - \varphi(or\ 90^o - 2\varphi)$ with respect to the surface slope $\partial\eta/\partial x$. This phase lag varies from small values (10° or 0.3 hours) in shallow, friction-dominated conditions (quasi-steady flow; velocity reacts directly to a decreasing water level in the direction of the flow) to about 90° in deep water (velocity responds delayed to water surface slope).

Figure 2 shows the velocity amplitude and the phase lead angle φ_1 (in hours) as a function of the water level amplitude at x=0 m for three water depth values h=5, 10, and 20 m in an open-end system (without reflection). The bed roughness (k_s) value is 0.05 m. The peak velocities (flood) at the mouth are in the range of 0.5–1.5 m/s for the smallest water depth of 5 m and in the range of 0.35–2.5 m/s for the largest depth of 20 m. The effect of the water depth is rather small. Roughly, the peak velocities (which are very realistic values for semi-diurnal estuaries) are in the range of 0.4–1.7 m/s for for $\widehat{n}_0$=0.5–3 m. The phase lead angles are between 1 and 1.4 hours for h=5 m and between 0.25 and 1 hour for h=20 m. The phase lead angle decreases with increasing depth (less bottom friction).

For a closed channel at one end, the solution represents a standing wave system characterized by incident and reflected waves of equal amplitude which individually propagate at speed c (smaller than the classical value $c_o=(gh_o)^{0.5}$), see Table 1. Resonance phenomena do occur when the channel length is of the order of 0.25 L with L=tidal wave length.

4.2 Convergent (funnel type) channels

The topography of most estuary channels is sufficiently complex that any realistic representation requires the division of the channel into a series of prismatic channels each with its own constant width b. The classical analytical approach is to

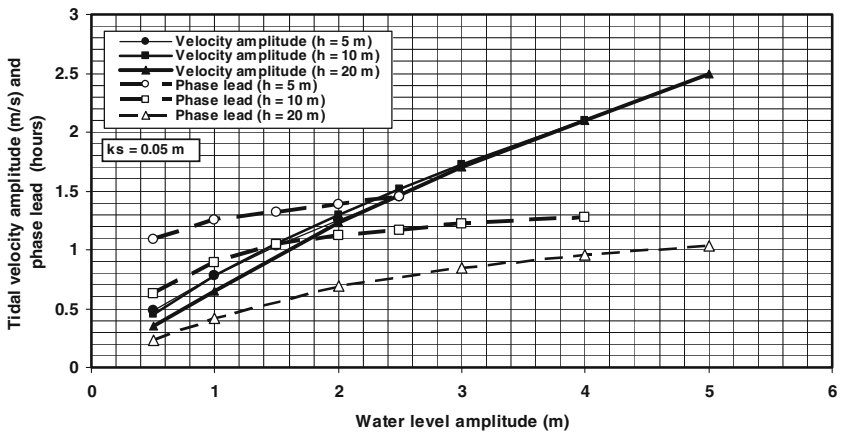

Fig. 2 Peak tidal velocity at mouth and phase lead angle as function of water level amplitude at mouth (0.5H) and water depth (negative flood velocity is plotted as positive value); prismatic channel without reflection

Author's personal copy

apply the equations for a *prismatic* channel to each channel section from seaward to landward direction using the output of the previous section as input for the next section (Dronkers 1964). Unfortunately, this method eliminates the large effect of channel convergence on the complex wave number and thus on the wave speed c (Jay 1991). Furthermore, this segment type of approach is laborious and offers no real advantage compared with a direct 1D numerical solution method.

Therefore, another approach is required which takes the channel convergence properly into account. This can be done by using an exponential function for the channel width allowing an analytical solution of the equations of continuity and momentum. The width of the channel is described by: $b = b_o e^{-\beta x}$ with $\beta = 1/L_b =$ convergence coefficient, L_b=converging length scale (constant in time). The analytical solutions with and without reflection are given in Table 1 (Van Rijn 2011).

The basic assumptions are: bottom is assumed to be horizontal, channel depth h_o to MSL is assumed to be constant in space and time, width is $b = b_o e^{-\beta x}$ with $\beta = 1/L_b =$ convergence coefficient, L_b=converging length scale, convective acceleration $\left(\overline{\overline{u}}\partial\overline{\overline{u}}/\partial x = 0\right)$ is neglected; linearized friction is used and x-coordinate is *positive in landward direction* and negative in seaward direction (flood velocity is positive and ebb velocity is negative).

The friction term is linearized as follows (Van Rijn 2011):

$$\frac{1}{A}\frac{\partial Q}{\partial t} + \frac{g}{}\frac{\partial \eta}{\partial x} + nQ = 0 \tag{10}$$

in which, n is a constant friction factor, $n = \left(8g\left|\widehat{Q}\right|\right)/(3\pi C^2 A^2 R)$.

The mass balance equation can be expressed as ($A =$ b h and $h = h_o + \eta$):

$$\frac{b\,\partial\eta}{\partial t} + \frac{b\,h_o\,\partial\overline{\overline{u}}}{\partial x} + \frac{\overline{\overline{u}}b\,\partial\eta}{\partial x} + \frac{\overline{\overline{u}}h_o\,\partial b}{\partial x} = 0 \tag{11}$$

The gradient of the width is $\partial b/\partial x = -\beta\ b_o\ e^{-\beta x} = -\beta\ b$. Neglecting the term $\overline{\overline{u}}b\partial\eta/\partial x$, the mass balance equation becomes:

$$\frac{\partial\eta}{\partial t} + \frac{h_o\partial\overline{\overline{u}}}{\partial x} - \overline{\overline{u}}\beta h_o = 0 \tag{12}$$

The momentum equation can be simplified to:

$$\frac{\partial\overline{\overline{u}}}{\partial t} + \frac{g\,\partial\,\eta}{\partial x} + m\,\overline{\overline{u}} = 0 \tag{13}$$

with $m = \mathrm{nA} = n\ b\ h_o = \left(8g|\widehat{\overline{u}}|\right)/(3\pi C^2 R) \cong \left(8g|\widehat{\overline{u}}|\right)/(3\pi C^2 h_o) =$ Lorentz friction parameter (dimension 1/s), $\overline{\overline{u}}$= cross-section-averaged velocity, $\widehat{\overline{u}}$=characteristic peak velocity (average value over traject), C=Chézy=coefficient, R= hydraulic radius. The river velocity $\overline{\overline{u}}_r = Q_r/A$ can easily be included. This leads to additional friction and more tidal damping.

In the case of a compound channel consisting of a main channel and tidal flats, it may be assumed that the flow over the tidal flats is of minor importance and only contributes to the tidal storage. The discharge is conveyed through the main channel. Inclusion of tidal flats in a 1D approach requires that the equations of continuity and momentum are modified to account for the different widths of the main channel and the flats (Van Rijn 2011). In Eq. 11, the multiplier of $\partial\eta/\partial t$ should be b_s (=surface width) rather than b resulting in $c_o = (\alpha_b\ g\ h_o)^{0.5}$ with $\alpha_b = b_c/b_s =$ width coefficient (in the range 0.5–1), b_c=width of main channel, and b_s=surface width. The transfer of momentum from the main flow to the flow over the tidal flats can be seen as additional drag exerted on the main flow (by shear stresses in the side planes between the main channel and the tidal flats). This effect can be included crudely by increasing the friction in the main channel through a smaller effective depth $h_{eff} = \alpha_h h_o$ with α_h in the range of 0.8–1 (to be used in the friction term). The width of the main channel and the surface width are both assumed to vary exponentially over the length of the channel (α_b=constant).

The (laborious) analytical solution based on complex functions is given by Van Rijn (2011) and is summarized in Table 1. The general solutions for k and μ are:

$$k = (2)^{-0.5}k_o\left[+1 - (0.5\beta/k_o)^2 + \left\{\left(-1 + (0.5\beta/k_o)^2\right)^2 + (m/\omega)^2\right\}^{0.5}\right]^{0.5} \tag{14}$$

$$\mu = (2)^{-0.5}k_o\left[-1 + (0.5\beta/k_o)^2 + \left\{\left(-1 + (0.5\beta/k_o)^2\right)^2 + (m/\omega)^2\right\}^{0.5}\right]^{0.5} \tag{15}$$

with $k_o = \omega/c_o$ and $c_o = (gh_o)^{0.5}$

Author's personal copy

This involves three cases (for details, see Van Rijn 2011):

Case A: Amplitude of water level and velocity are constant (ideal estuary or synchronous) $H=H_o$ $\beta = 2\omega/c_o = 2k_o$ or $1/L_b = 2k_o$ and $c=c_o=(gh_o)^{0.5}$; convergence and friction are about equal.

Case B: Amplification is dominant (hypersynchronous) $H>H_o$ with $\beta \geq {}^3 2\omega/c_o$ or $1/L_b > 2k_o$ and $c>c_o$; inertia and convergence dominate bottom friction

$$k = 0.5^{0.5}(\omega/c_o)\alpha^{0.5}\left[-1+\left\{1+m^2/\left(\omega^2\alpha^2\right)\right\}^{0.5}\right]^{0.5}$$
$$\text{with } \alpha = 0.25\beta^2(c_o/\omega)^2 - 1$$
$$k = 0.5^{0.5}(k_o)\alpha^{0.5}\left[-1+\left\{1+m^2/\left(\omega^2\alpha^2\right)\right\}^{0.5}\right]^{0.5} \quad (16)$$
$$\text{with } \alpha = 0.25\beta^2(1/k_o)^2 - 1 \text{ and } k_o = \omega/c_o$$

$$\mu = (m\omega)/\left(2c_o{}^2\right)(1/k) \quad (17)$$

μ can also be expressed as:

$$\mu = 0.5^{0.5}(\omega/c_o)\alpha^{0.5}\left[1+\left\{1+m^2/\left(\omega^2\alpha^2\right)\right\}^{0.5}\right]^{0.5}$$

The actual propagation velocity or phase velocity c can be expressed as:

$$c = \frac{L}{T} = \frac{\omega}{k} = \frac{c_o}{(0.5\alpha)^{0.5}(-1+a_2)^{0.5}} \quad (18)$$

with: $a_2 = [1 + m^2/(\omega^2\alpha^2)]^{0.5}$

This latter expression yields a wave propagation velocity larger than that of a frictionless wave ($c>c_o$). Practical values, $a_2 \cong 2$–3.

Tidal amplification is dominant in deep estuaries with strong width reduction (strong convergence).

The tidal amplification is fairly linear. In short estuaries, a near-standing wave pattern can be generated with a phase lead close to 3 hours (relatively large "apparent" wave speed).

Observations in amplified estuaries also show that the real wave speed (c) is larger than the classical value ($c_o=(gh_o)^{0.5}$). The observed wave speed in the Scheldt Estuary is about 13–16 m/s, whereas $c_o=(gh_o)^{0.5}$ is of the order of 10 m/s.

Case C: Damping is dominant (hyposynchronous) $H<H_o$ with $\beta \leq 2\omega/c_o$ or $1/L_b < 2k_o$ and $c<c_o$; bottom friction dominates inertia and convergence.

$$k = 0.5^{0.5}(\omega/c_o)\alpha^{0.5}\left[1+\left\{1+m^2/\left(\omega^2\alpha^2\right)\right\}^{0.5}\right]^{0.5}$$
$$\text{with } \alpha = 1 - 0.25\beta^2(c_o/\omega)^2$$
$$k = 0.5^{0.5}(k_o)\alpha^{0.5}\left[1+\left\{1+m^2/\left(\omega^2\alpha^2\right)\right\}^{0.5}\right]^{0.5}$$
$$\text{with } \alpha = 1 - 0.25\beta^2(1/k_o)^2 \text{ and } k_o = \omega/c_o \quad (19)$$

$$\mu = (m\omega)/\left(2c_o{}^2\right)(1/k)$$
μ can also be expressed as : (20)
$$\mu = 0.5^{0.5}(\omega/c_o)\alpha^{0.5}\left[-1+\left\{1+m^2/\left(\omega^2\alpha^2\right)\right\}^{0.5}\right]^{0.5}$$

The actual propagation velocity c is:

$$c = \frac{L}{T} = \frac{\omega}{k} = \frac{c_o}{(0.5\alpha)^{0.5}(1+a_2)^{0.5}} \quad (21)$$

with $a_2 = (1 + m^2/(\omega^2\alpha^2))^{0.5}$

This latter expression yields a wave propagation velocity which is smaller than that of a frictionless wave ($c<c_o$). Practical values, $a_2 \cong 1$–5.

In an *ideal* (*synchronous*) estuary, the tidal range H remains constant and the wave speed c is equal to $c_o=(gh_o)^{0.5}$. Basically, the convergence process (increase of potential energy) is balanced by the damping process (energy dissipation by friction). The tidal range H remains constant, if the exponent (see Table 1):

$$-0.5\beta + \mu = 0 \text{ or } \beta = 2\mu \text{ or } L_b = 1/(2\mu),$$
$$\text{with } 2\mu = (2m\omega)/\left(2kc_o{}^2\right) = mc/c_o{}^2 = m/c_o$$
$$\text{Thus, } L_b = 1/\beta = 1/(2\mu) = c_o/m$$

Using: $m = \left(8g|\widehat{\overline{u}}|\right)/(3\pi C^2 h_o) = (f|\widehat{\overline{u}}|)/(3\pi h_o) =$ Lorentz-friction parameter; $\widehat{\overline{u}}_o = (0.5H/h_o)c\ \cos(\varphi)$, it follows that: $L_b = (6\pi\ h_o)/(f\ \gamma\ \cos\varphi)$ with: $\gamma = H/h_o$. Since $\mu=k$ for an ideal estuary, it is also valid that $L_b = 1/(2k) = L_{wave}/(4\pi)$. This approach leads to the same converging length scale L_b as that based on Eq. 6 (at end of section 3). Similarly ($f \cong 0.025$ and $\cos\varphi \cong 0.7$), the length of the synchronous part of an alluvial estuary is about $L \cong 2L_b \cong 2,000(h_o/H)h_o$.

Table 1 shows a transparent set of equations for prismatic and converging channels. They are almost similar except for one coefficient $\beta = 1/L_b$ (e-folding length scale parameter for the channel width). It can be immediately seen that the equations for converging channels reduce to that for prismatic channels, if the length scale L_b goes to infinity and thus β goes to zero.

To better understand the response of the velocity to the water level variation and the phase shifts involved in a strongly converging estuary, it should be realized that the velocity is governed by surface slope ($\partial\eta/\partial x$), bottom friction, inertia $\left(\partial\overline{\overline{u}}/\partial t\right)$ and the converging width.

The water surface slope can be expressed as:

$$\partial\eta/\partial x = \widehat{\eta}_o\left[e^{(-0.5\beta+\mu)x}\right]\left[\left((0.5\beta-\mu)^2+k^2\right)^{0.5}\right]\cos(\omega t - kx + \psi)$$
$$\text{with } \tan\psi = k/(0.5\beta-\mu) \text{ for } (0.5\beta-\mu) > 0 \text{ (weakly converging estuary)}, \quad (22)$$

Author's personal copy

or

$$\partial\eta/\partial x = \eta_o\left[e^{(-0.5\beta+\mu)x}\right]\left[\left((0.5\beta-\mu)^2+k^2\right)^{0.5}\right] \times \cos(\omega t - kx + 180^o - \psi) \quad (23)$$

with: $\tan\psi = k/(\mu - 0.5\beta)$ for $(0.5\beta-\mu)<0$ (strongly converging estuary).

The phase lag of the velocity to the water surface slope is $\psi-\varphi$.

Practical values of these phase lags are (h_o=10 m, k_s=0.05 m, T=12.5 h);

strongly converging estuary with L_b=10,000 m, $\varphi\cong90°$, $\psi\cong150°$, and $\psi-\varphi\cong60°$(≅2 h),

weakly converging estuary with L_b=50,000 m: $\varphi\cong50°$, $\psi\cong85°$, and $\psi-\varphi\cong30°$ (≅1 h).

Figure 3 shows a plot the ratio $\beta/(2\mu)$, relative phase speed c/c_o and phase shift φ (in hours) as a function of the parameter L_b/h_o. This latter parameter expresses the ratio of the width converging parameter (L_b) and the water depth (h_o). This parameter L_b/h_o is used because it can easily be determined from the planform (Google Earth) and bathymetric charts. L_b is the length over which the width at the mouth is reduced by about 35%. The present results are based on practical depths of h_o=10 and 5 m; and L_b values in the range of 10–100 km. The ratio $\widehat{\eta}_o/h_o$=0.2. The width at the mouth is b_o=25 km. The k_s value is k_s=0.03 m.

The parameter $\beta/(2\mu)$ expresses the behavior of the tidal wave (amplification or damping). An *ideal* estuary with a constant tidal range is present for $\beta/(2\mu)$=1. Larger values of $\beta/(2\mu)$ for a strongly converging estuary (L_b/h_o<4,500) yield an amplified estuary and smaller values of $\beta/(2\mu)$ lead to a damped estuary (L_b/h_o>4,500). The ratio of the wave speed (c) and the frictionless wave speed (c_o) is in the range of 10 for a strongly converging estuary to 0.8 for a weakly converging estuary. The phase lead φ is about 3 h in a very strongly converging estuary and about 1 h in a weakly converging estuary.

The results of Fig. 3 show that the wave speed in a strongly convergent channel with L_b/h_o in the range 1,000–3,000 is much larger than the classical value of $c_o=(gh_o)^{0.5}$. Thus, c/c_o>1. The phase lead φ between the horizontal ($\overline{\overline{u}}$) and vertical tide (η) is in the range of 2–3 h and is strongly influenced by the geometrical parameters (L_b/h_o) in sharp contrast to the classical description of a frictionally damped wave in a prismatic channel. The wave system in a strongly convergent channel seems to mimic a standing wave system. According to Friedrichs and Aubrey (1994), convergent estuaries represent an asymptotic solution for which it is not necessary to calculate the reflected wave in a channel of finite length outside the immediate vicinity of the close end. According to Le Floch (1961), this only applies to a channel of infinite length and thus in a real estuary, it is always necessary to include the wave reflected at the closed end of the channel. However, the reflected wave will propagate in a divergent channel (widening channel in seaward direction) causing rapid damping of the wave due the lateral spreading of energy and due to bottom friction. Reflection effects will be confined to a region with a length scale of the order of the e-folding length scale (L_b) or less, which is in the range of 10–30 km for most estuaries.

The solution for a closed-end channel including the reflected wave is given in Table 1 (see Van Rijn 2011). The reflected wave decreases in height due to divergence (widening) of the channel, which means that the sign of the β-coefficient is opposite for the reflected wave. Thus, the reflected wave is damped due to channel divergence and friction (the incoming wave is amplified by convergence and damped by friction).

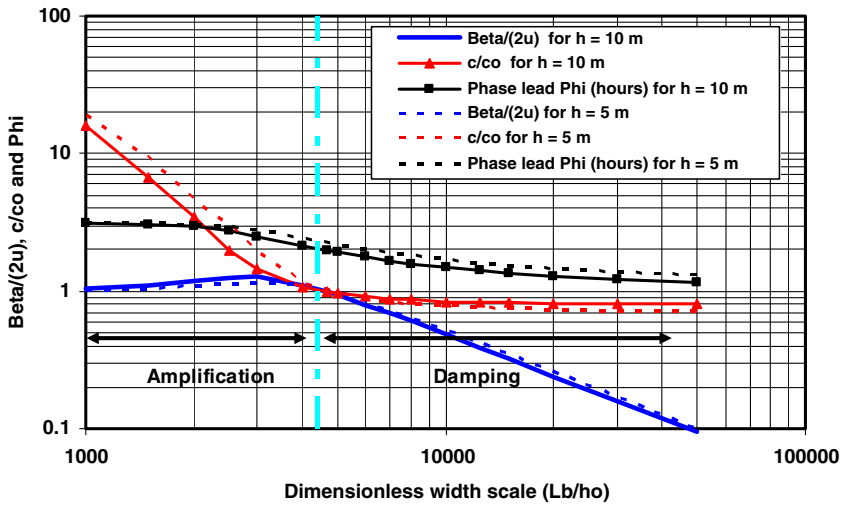

Fig. 3 Amplification and damping in a funnel-type estuary (exponential width)

Author's personal copy

4.3 Numerical solutions

The most universal solution of the equations of continuity and momentum including nonlinear terms and reflection can only be obtained by using numerical models, using either a 1D cross-section-averaged approach or a 2DH depth-averaged approach. Herein, the results of the DELFT1D-model (SOBEK) and the DELFT2DH-model of Deltares/Delft Hydraulics are presented for various schematized cases with boundary conditions as present in the Western Scheldt Estuary (The Netherlands). The water levels are computed in the nodal points and the velocities (discharges) in the reaches between the nodes. Both models yield values which are in reasonable agreement (within 5–15%). The numerical results are compared to those of the analytical models.

5 Applications

Three large-scale estuaries with semi-diurnal tides have been selected: the Western Scheldt Estuary (mesotide) at the border between The Netherlands and Belgium, the Hooghly Estuary (macrotide) in India, and the Delaware Estuary (microtide) in the USA. These estuaries represent a range from shallow (Delaware) to deep (Western Scheldt) estuaries. The tidal range at the mouth varies from micro (Delaware) to macro (Hooghly), see Davies (1964). Furthermore, the bottom roughness varies from a smooth muddy bed (Hooghly) to a rough bed with sand ripples and dunes (Western Scheldt)

5.1 Western Scheldt Estuary

All methods have been applied to the Western Scheldt Estuary in the southwest part of the Netherlands and in the northwest part of Belgium. It provides access to the port of Antwerp in Belgium, requiring rather large channel depths to allow passage of large vessels. The length of the estuary is about 60 km (up to Bath). The estuary including the tidal river has a total length of about 180 km (up to Gent, Belgium) and has the following characteristics: $b_o \cong 25$ km (=width at mouth), $\widehat{u}_o \cong 1.2$ m/s (peak velocity at mouth), $h_o \cong 10$ m (=depth at mouth), $H_o = 4.2$ m (=tidal range at mouth), $C \cong 55$–60 m$^{0.5}$/s or $f = 0.018$–0.026 ($k_s \cong 0.03$–0.1 m), $T \cong 12$ h, $\varphi \cong 75° \cong 2.5$ h, The small river discharge (about 100 m^3/s) has been neglected. The bottom is almost horizontal up to $x = 80$ km. Measured tidal data during spring tide at various stations in the Netherlands are shown in Table 2 (based on De Kramer 2002).

The width of the estuary is represented by an exponential function with a convergence length scale parameter of the order of $L_b \cong 25$ km (giving widths of 7.5, 2.5, and 1 km at Terneuzen, Bath, and Antwerpen in agreement with measured data, see Table 2) and $\beta = 1/25{,}000 \cong 0.00004$. Two values of the bottom roughness height have been used ($k_s = 0.01$ and 0.05 m). The cross-section is assumed to be rectangular.

The measured tidal data at various stations in the estuary (Table 2) show an amplication factor of the tide of about 1.4 for springtide between the Station Westkapelle (mouth $x = 0$) and Station Antwerpen.

The energy-based method (see Eq. 6) involves the parameters $\widehat{u}$ and φ, which are taken from the linearized solution (Table 1; spreadsheet model tidalmotion.xls) for a funnel-type estuary. The computed tidal range values for a depth of 10 m and two bottom roughness values are shown in Fig. 4. The computed values are close to the measured values up to Station Hansweert at about 45 km from the mouth, but are too small in the landward part of the estuary where reflection plays a role as indicated by the measured data (between Bath and Antwerp the tidal ranges are relatively high). These amplification values show that width convergence dominates over bottom friction in the Western Scheldt up to Antwerp.

Figure 5 shows the measured and computed tidal ranges along the estuary based on the analytical linearized solution (without reflection). The k_s values are in the range of 0.03–

Table 2 Measured tidal data (spring tide) of Western Scheldt Estuary

Stations	Distance x (km)	Width b (km)	Tidal range H (m)	H/H_o (measured)
Westkapelle (mouth)	0	25	4.2 (=H_o)	1
Vlissingen	12	6	4.5	1.07
Terneuzen	30	6	4.8	1.14
Hansweert	45	6	5.0	1.19
Bath	63	3	5.5	1.31
Antwerpen	95	0.8	5.85	1.39
Rupelmonde	110	<0.5	5.95	1.42
Temse	115	<0.5	5.85	1.39
Dendermonde	130	<0.5	4.2	1.0
Gent	160	<0.5	2.34	0.55

Author's personal copy

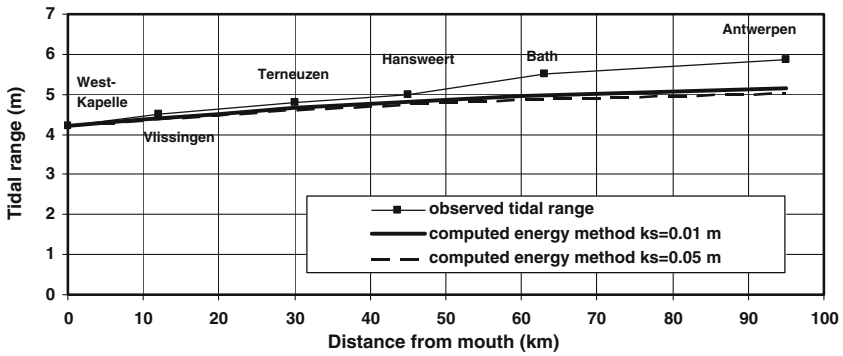

Fig. 4 Observed and computed tidal range along Western Scheldt Estuary (h=10 m); energy-based method

0.1 m and the L_b is in the range of 20–30 km. The computed wave speed is about 19–17 m/s for these roughness values, which is somewhat larger than the measured data in the range of 13–16 m/s between the mouth and station Bath at about 60 km from the mouth (Savenije 2005). The phase lead is about 2.7 h, which is somewhat larger than the observed value of about 2 h. The peak tidal velocities at the mouth are in the range of −0.75 to −0.85 m/s.

The computed values (without reflection; open end) are in good agreement (within 10%) with the observed values. A larger k_s leads to a smaller tidal range. The tidal amplification is somewhat too small for larger k_s values. A larger L_b leads to less amplification.

Figure 5 also shows results of the numerical solution method (with and without reflection). The numerical results with reflection are based on a closed channel at Antwerp (x=95 km).The numerical results without reflection are based on an open end at Antwerp by extending the channel (from Antwerp at 95 km) to about 180 km. The width at the end of the (closed) channel is set to 100 m. The numerical model results show that reflection yields an important contribution in the landward half of the Western Scheldt Estuary. The geometry of the relatively wide landward end of the estuary with the small-scale Scheldt river entering the estuary is such that significant reflection may occur. Comparing the results of the linearized model (without reflection at the closed channel end) and the results of the numerical model without reflection, it is clear that the linearized model produces values which are substantially larger. The analytical model including reflection produces values which are much too large (not shown).

The depth of the navigation channel to the Port of Antwerp in Belgium is a problematic issue between The Netherlands and Belgium because of conflicting interests (commercial versus environmental). Large vessels require a deep tidal channel to Antwerp, which enhances tidal amplification with negative environmental consequences. Thus, it is of prime importance to know the proper relationship between the water depths and the tidal amplification. Figure 6 shows the ratio ($H_{x=60\mathrm{km}}/H_o$) of the tidal range at x=60 km (end of estuary section near Belgium border) and at the entrance x=0 as a function of the water depth (in the range of 5–20 m) based on various methods for a bottom roughness value of k_s=0.05 m.

The energy-based method shows tidal damping due to bottom friction resulting in $H_{x=60\mathrm{km}}/H_o<1$ for water depths smaller than about 7 m. The tidal range shows amplification (>1) for water depths larger than about 7 m. The maximum amplification based on the energy equation with quadratic friction is about 1.2 at a water depth of about 11 m. A further increase of the depth does not lead to larger

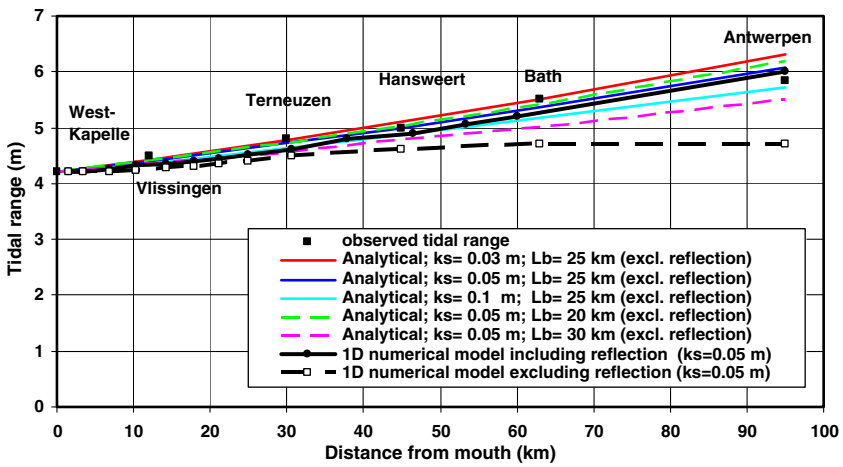

Fig. 5 Observed and computed tidal range along Western Scheldt Estuary (h=10 m)

Author's personal copy

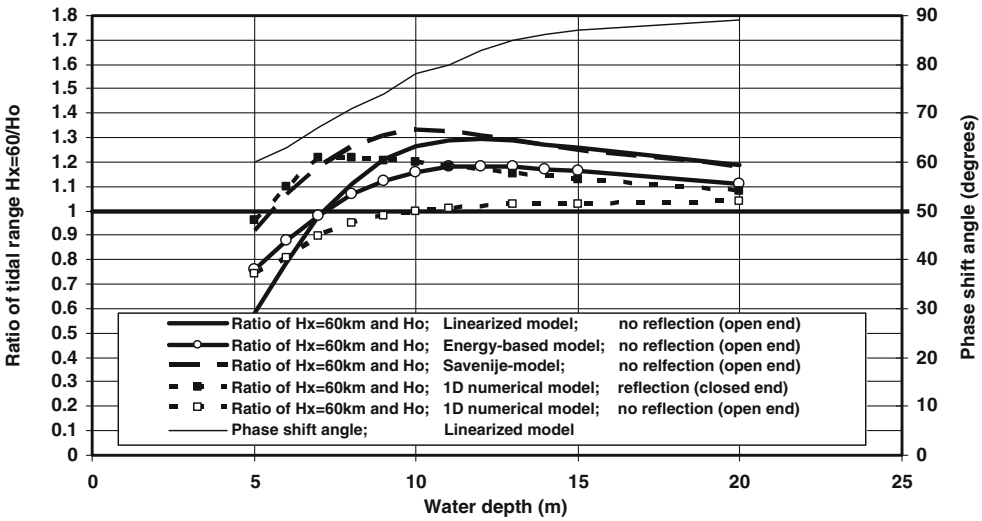

Fig. 6 Ratio $H_{x=60\ \mathrm{km}}/H_{\mathrm{o}}$ as function of water depth for Western Scheldt Estuary (k_s=0.05 m)

amplification values. The maximum amplification based on the linearized solution of the mass and momentum balance equations is about 1.3. The computed phase angle φ based on the linearized solution is also shown. The phase angle φ gradually increases from 60° (about 2 h) at a depth of 5 m to about 90° (about 3 h) at a depth of 20 m. Thus, it approaches a value of 90° for larger depths, which is close to the phase lead of a standing wave system. So, the progressive tidal wave in a strongly, convergent estuary behaves as a (apparent) standing wave, although the reflected wave is not considered.

All analytical methods produce similar results for a very deep channel, in which bottom friction is small. The models differ for shallow channels due to the different representation of bottom friction. The energy-based method including quadratic friction is more accurate than the linearized model. The model of Savenije (2005) also includes quadratic friction, but its derivation based on a Lagrangian approach, is not very transparent and may involve inconsistencies.

The results of the numerical DELFT1D-model taking all terms into account are also shown, both for a channel with a closed end (with reflection) and an open end (no reflection). The results of the numerical model show a significant effect of reflection at the channel end. The results of all analytical methods (without reflection) are considerably larger (overprediction) than the numerical results without reflection for water depth larger than about 10 m. The Savenije model shows overprediction over the full range of water depths.

Figure 7 shows the effect of the bed roughnes (k_s=0.05 and 0.001 m) on the tidal amplification factor ($H_{x=60\ \mathrm{km}}/H_{\mathrm{o}}$) based on the energy Eq. 6 for a channel with a rectangular cross-section. A smaller k_s value leads to a larger amplification factor for depths smaller than 15 m. Friction has almost no effect for depths larger than about 15 m (convergence is dominant).

The analytical models are most valid for a rectangular cross-section. Real converging tidal channels, however, have a compound cross-section with one or more deeper channels with shallow flats or floods plains in between and along the banks.

To evaluate the effect of the cross-section on the computed water levels, various computations have been made for a compound cross-section consisting of one main channel and

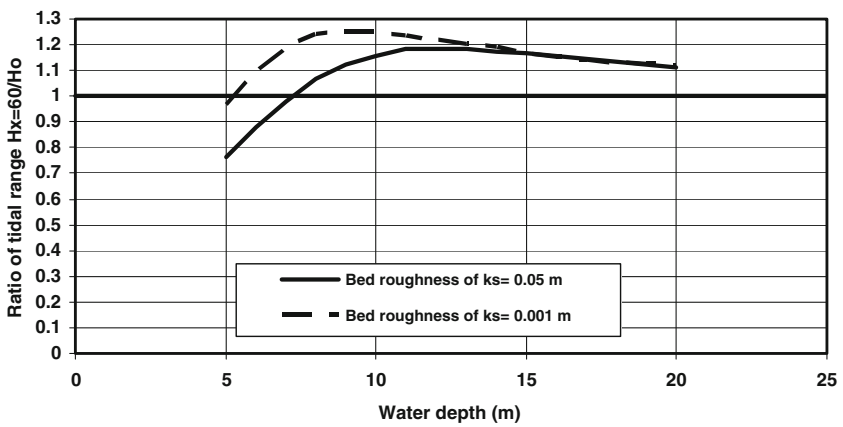

Fig. 7 Ratio $H_{x=60\ \mathrm{km}}/\mathrm{H_o}$ based on energy method; effect of k_s

Author's personal copy

tidal flood plains using the 1D numerical model and both analytical models (energy-based model and linearized model). The results are compared to those for a converging channel with a rectangular cross-section. A converging channel with an open end (no reflection) has been considered only. The width at the mouth is $b_{s,o}$=25,000 m. The analytical models have also been applied; the effect of the cross-section is taken into account by using the hydraulic radius in the friction term and the effective channel depth for the wave speed. The wave speed was also computed by using the hydraulic radius (alternative method).

The compound cross-section is assumed to consist of one main channel and tidal flats on both sides; the width of the main channel at the mouth is $b_{c,o}$=10,000 m and h_{flats}= 3 m, the total width of the flats is b_{flats}=15,000 m, the total width at the mouth is $b_{s,o}$=25,000 m. The depth of the main channel (compound cross-section) is h_c=h_o. The width of the main channel is b_c. The total surface width is b_s. The effective wave propagation depth of the main channel is defined as $h_{eff}=A_c/b_s=(b_c/b_s)h_o$ with A_c=area of main channel. The hydraulic radius is $R\cong A/b_s$ with A=area of total cross-section. The width at the mouth of the rectangular cross-section is $b_{s,o}$=25,000 m.

For example, a compound cross-section with $h_c=h_o$= 20 m, h_{flat}=3 m, b_s=25,000 m, b_c=10,000 m has an effective depth of h_{eff}=8 m and a hydraulic radius of R= 9.8 m. It is noted that the representation of a compound channel by using the concept of hydraulic radius to represent the frictional depth and the wave propagation depth is questionable. Based on this concept, the bed–shear stresses is distributed evenly along the wet perimeter of the cross-section.

Figure 8 shows the effect of the cross-section on the ratio $H_{x=60km}/H_o$ based on various models. The analytical results of the linearized model and the energy-based model show that significant amplification only occurs in a compound channel when the depth of the main channel is relatively large (h_o>15 m). For example, a *compound* cross-section with a channel depth of 20 m and an effective depth of 9.8 m (equal to hydraulic radius) has an analytical amplification factor of 1.25 (see Fig. 8), which is exactly equal to that of a *rectangular* cross-section with a depth of 9.8 m. This value (amplification=1.25) is somewhat larger than that (amplification=1.18) of a rectangular channel with a depth of 20 m. If the main channel depth is larger than about 25 m, the amplification factor based on the analytical results gradually decreases.

The numerical model results show tidal damping for water depths smaller than about 10 m, both for a rectangular and a compound cross-section. The tidal damping is largest for a compound channel. The differences are largest for smaller depths. The numerical model results only show slight amplification for larger water depths (maximum, 1.15). The results of the 1D and 2DH numerical models show reasonably good agreement for a channel with a compound cross-section, which puts some confidence on the simple 1D concepts.

The analytical results of the energy-based model for a compound cross-section are in reasonable agreement with the numerical results for water depths smaller than 13 m.

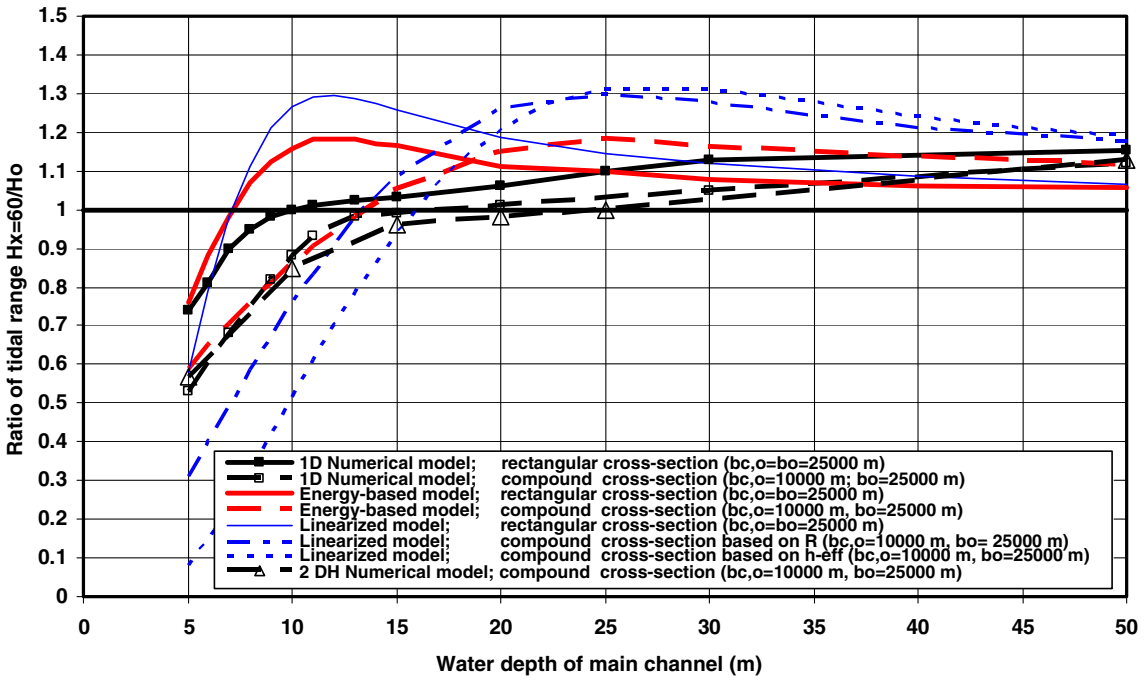

Fig. 8 Ratio $H_{x=60\ km}/H_o$ for Western Scheldt Estuary; effect of cross-section

Author's personal copy

The analytical results of the energy-based model are slightly overpredicted for water depths between 15 and 30 m. The analytical results of the linearized model for a compound cross-section are too small compared with the numerical results for water depths smaller than about 13 m, particularly if the effective wave propagation depth is used. Better agreement with the numerical model results is obtained if the effective wave propagation depth is represented by the hydraulic radius for $h<13$ m. The analytical results of the linearized model are significantly overpredicted for water depths between 10 and 30 m (compound cross-section).

It is noted that the assumption of tidal flats with a total width of 15,000 m at the mouth (60% of total width) is an extreme case which does not apply to the Western Scheldt Estuary, where the contribution of the tidal flats is not more than about 10%. Using relatively small tidal flats, the computed tidal range (analytical model) is not significantly affected (not shown). Based on this, the effect of the tidal flats on the amplification of the tidal range is found to be marginal for the Western Scheldt Estuary and thus the cross-section can be reasonably well represented by a rectangular cross-section.

5.2 Hooghly Estuary

The large-scale Hooghly Estuary in the State of West Bengal drains the Hooghly–Bhagirathi River system. The river derives its upland discharge from the Ganga during monsoons. The bed consists of fine sediments (silt–mud range). It is a tidal system over 290 km from the mouth. The port of Calcutta is on the left bank of the river at about 150 km from the mouth. The water depth to mean sea level is about 6–8 m up to Calcutta.

The width of the mouth is about 22 km and the L_b length scale is about 25 km ($\beta=1/25{,}000=0.00004$).

The observed spring tidal range (semidiurnal) show tidal amplification over about 0–100 km and tidal damping over 100–290 km (see Fig. 9).

To apply the analytical linearized model (spreadsheet model Tidalmotion.xls), the total channel traject has been divided into two parts: a converging section over about 100 km and a prismatic river section over about 200 km. The following data have been used to compute the tidal range over 300 km. The river discharge has been neglected.

Converging section 0–100 km; $h_o=7$ m, $b_o=22{,}000$ m, $L_b=25{,}000$ m, $\widehat{\eta}_o=2.35$ m, $T=45{,}000$ s,

Prismatic section 100–300 km; $h_o=7$ m, $b_o=400$ m, $L_b=500{,}000$ m, $\widehat{\eta}_o=\widehat{\eta}_{x=100\ \mathrm{km}}$, $T=45{,}000$ s.

Three bottom roughness values have been used; $k_s=0.005$, 0.01, and 0.03 m.

The computed characteristic parameters for $k_s=0.005$ m are $\omega=0.00014$ (1/s), $m=0.000237$ (1/s), $c_o=8.29$ m/s, $c=10.1$ m/s, $k=1.38\,10^{-5}$ (1/m), $\mu=1.75\,10^{-5}$ (1/m), and $\varphi=2.42$ h (73°).

The results (Fig. 9) show that the computed tidal amplification is in close agreement with the observed values for a small roughness value of $k_s=0.005$ m (5 mm), which is quite realistic for a silt–mud estuary. The tidal amplification is much too small for larger k_s values. The model yields tidal damping over the traject from 100 to 300 km for $k_s=0.005$ m in agreement with the observations. The computed length of the tidal penetration is in good agreement with the observed data. Overall, the computed tidal ranges are within 15% of the observed data for a k_s value of 0.005 m.

The friction coefficient is $f=g/C^2\cong 0.0015$ for $C\cong 75\ \mathrm{m}^{0.5}/\mathrm{s}$. Prandle (2003a, b) reports friction coefficients in the range of 0.001 (mud content of about 90%) to 0.004 (mud content of 20%) for muddy estuaries, based on analysis of a range of estuaries. He proposes: $f=0.073/M$ with M=percentage of mud. Using $f=0.0015$, the mud content would be about 50% for the Hooghly estuary, which is quite realistic.

Figure 10 shows the tidal water level and velocity variation at $x=50$ km and at the mouth ($x=0$) for $k_s=0.005$ m. The flood velocity is positive. The phase shift of HW is about 1.5 h over 50 km. The peak flood velocity at x

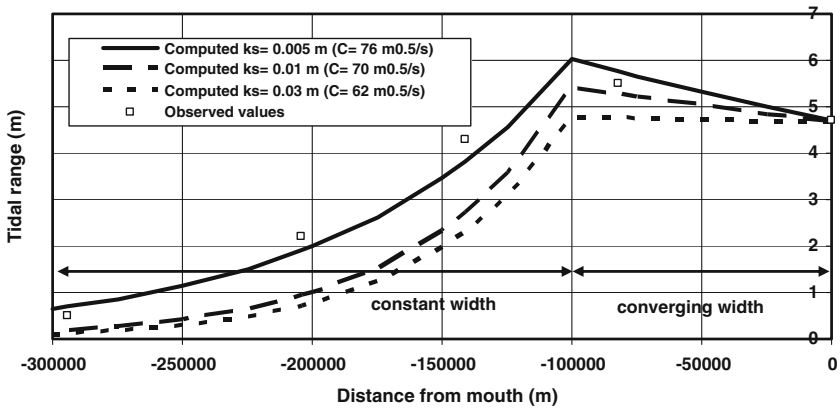

Fig. 9 Measured and computed tidal range values, Hooghly Estuary; linearized method

Author's personal copy

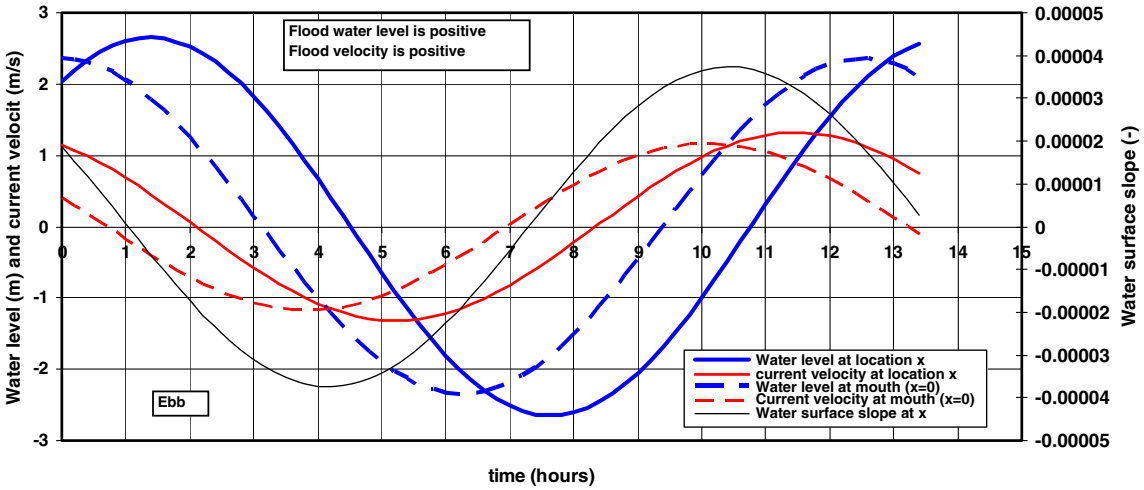

Fig. 10 Water level and velocity at x=50 km and at x=0 m for k_s=0.005 m, Hooghly Estuary

=50 km occurs about 2.4 h before the time of HW at x= 50 km. The phase shift between the horizontal and vertical tide is about 2.4 h, which is in good agreement with the value of 2.5 h (about 75°) for a depth of about 7 m and tidal amplitude of about 2 m presented by Prandle (2003a, b; Fig. 7). The water surface slope at x=50 km is also plotted. The velocity at x=50 km has phase lag of about 1 h with respect to the water surface slope.

5.3 Delaware Estuary

The Delaware Estuary (USA) is a funnel-shaped estuary extending from Cape May on the Atlantic coast to the fall line at Trenton, a distance of about 210 km along the axis of the estuary (Harleman 1966). The width varies from approximately 40 km at the widest portion of Delaware Bay to approximately 300 m at Trenton. Using an exponential width variation, the length scale is approximately L_b=45 km. The mean depth is approximately 6.1 m. The tidal range at the ocean entrance is about 1.3 m and increases to 1.8 m at Woodland Beach, decreases to 1.6 m at Edgemoor and increases again to a maximum of about 2 m at Trenton (Delaware river). The time of high water at Trenton is almost 8 h later than at the ocean entrance.

Figure 11 shows observed and computed tidal range values (without reflection) over a total distance of 210 km from the entrance to Trenton. The bed roughness values were obtained by calibration resulting in values in the range of k_s=0.005 m to 0.03 m (C=75 to 61 $m^{0.5}$/s or f=0.014 to 0.021). The best results are obtained for k_s=0.01–0.02 m. The damping coefficient is $\mu \cong 0.00001$. The computed phase shift between the horizontal and vertical tide is about 1.9 h. The peak tidal velocity near the entrance is about 0.52 m/s giving a discharge of about 135,000 m^3/s. Harleman reports discharge values of 35,000 m^3/s at about 60 km from the entrance (150 km from Trenton). The computed value at that location is about 36,000 m^3/s for k_s=0.01 m, which is close to the measured value. The

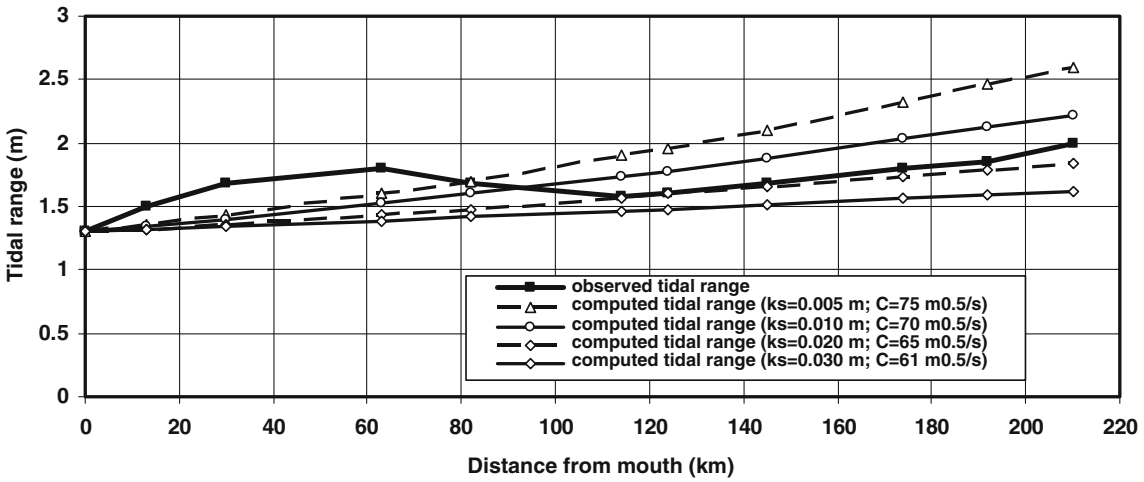

Fig. 11 Measured and computed tidal ranges, Delaware Estuary, USA; linearized method

Author's personal copy

measured peak discharge at a distance of about 25 km from Trenton (185 km from entrance) is 1,900 m^3/s. The computed value is about 2,350 m^3/s. The computed wave speed is 8.7 m/s which is somewhat larger than the frictionless value of 7.9 m/s. Computed HW at Trenton is about 6.5 h later than that at the entrance (observed 8 h). Hence, the observed wave speed is 210 km/8 h=7.3 m/s which is somewhat smaller than the frictionless value. The bulgy type of behavior of the measured tidal curve between x=0 and 100 km from the entrance (see Fig. 11) cannot be represented by the relatively simple geometrical schematization with an exponential width variation, a constant depth, and one tidal constituent (M_2). A better representation requires numerical modeling taking the actual width and depth variations into account and harmonic tidal analysis to produce more detailed tidal boundary conditions at the entrance.

6 Intercomparison of numerical and analytical results for converging channels

The analytical linearized method and the numerical methods have been intercompared systematically for converging tidal channels.

The following six cases of converging channels with tidal motion have been used (see Fig. 12):

Case 1: Converging width over 60 km (width b_o= 25,000 m, $b_{L=60\ km}$=2000 m), depth h=10 m, k_s=0.05 m

Case 3: Converging width over 60 km (width b_o= 25,000 m, $b_{L=60\ km}$=2,000 m), depth h=5 m, k_s=0.05 m

Case 2: Converging width over 60 km (width b_o= 25,000 m, $b_{L=60\ km}$=2,000 m) constant width (prismatic) over 60–180 km (b=2,000 m), depth h=10 m, k_s=0.05 m

Case 4: Converging width over 60 km (width b_o= 25,000 m, $b_{L=60\ km}$=2,000 m) constant width (prismatic) over 60–180 km (b=2,000 m), depth h=5 m, k_s=0.05 m

Case 5: Converging width over 180 km (width b_o=25,000 m, $b_{L=60\ km}$=19 m), depth h=10 m, k_s=0.05 m

Case 6: Converging width over 180 km (width b_o=25,000 m, $b_{L=60\ km}$=19 m), depth h=5 m, k_s=0.05 m

with b_o=width at mouth, b_L=width at end of channel, and L_b=converging width length scale=25,000 m. The width

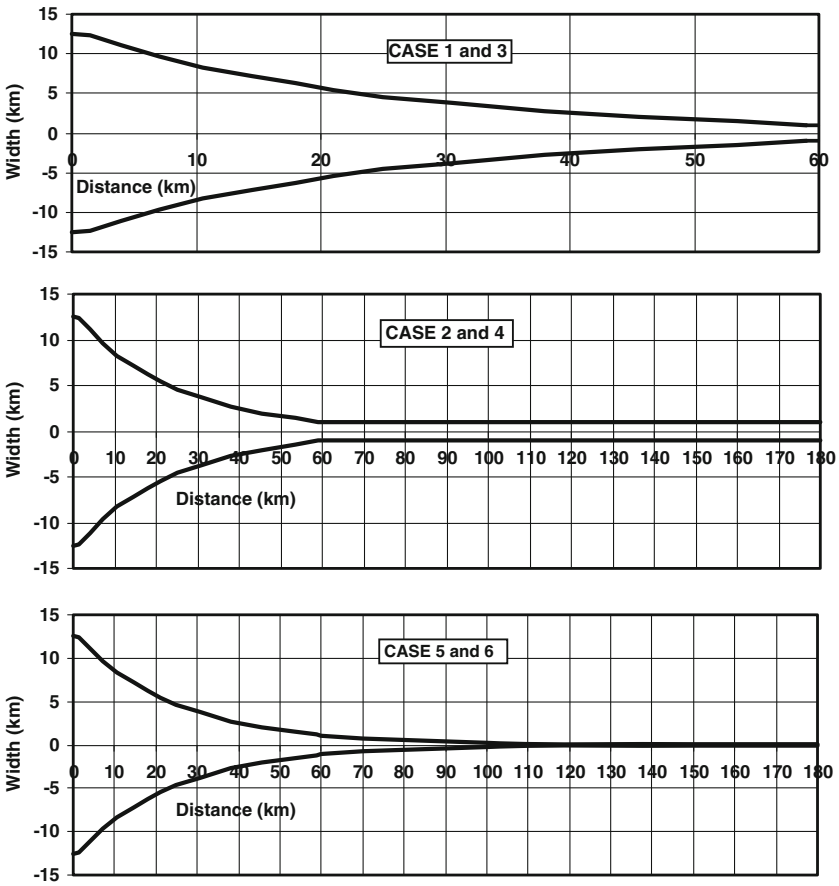

Fig. 12 Width of converging channel (cases 1–6)

Author's personal copy

parameters of the converging section between 0 and 60 km are based on Western Scheldt data.

Mouth (x=0): water level amplitude, $\eta=\widehat{\eta}\cos(\omega t)$ with $\widehat{\eta}$=2.1 m, and $\omega=2\pi/T$, T=12 h,

water level variation is represented by hourly values,

Closed end ($x=L$), discharge Q=0 m^3/s

The constant water depth is defined as the depth to MSL; tidal levels are defined to MSL.

Figure 13 shows the computed tidal range values for cases 1–6 based on the numerical model results (DELFT2DH). Amplification can be observed for a deep channel with a converging width over the entire channel length (cases 1 and 5). Wave reflection does occur at the landward end. Slight damping of the tidal range due to bottom friction can be observed for a shallow channel with a fully converging width. The damping of the tidal range is considerably larger when the width remains constant after 60 km (cases 2 and 4).

Figure 14 shows the computed tidal range along the channel for cases 1 and 3 based on the three models applied. The analytical model has been applied with and without reflection at the closed channel end. All models predict amplification due to the width convergence and reflection at end for case 1 with a short channel length of 60 km and a mean water depth of h=10 m. Inclusion of reflection in the analytical model leads to a strong over-estimation of the tidal range in the landward half of the channel (about 30 km). Linear friction is too small to generate sufficient damping of the wave in this part of the channel. Exclusion of reflection yields almost perfect agreement of the analytical model results with the numerical model results. The computed wave propagation speed according to the analytical model is about 17 m/s (without reflection) and about 12 m/s (with reflection) for case 1, which is significantly larger than the classical value of $c=(g\,h_o)^{0.5}\cong$ 10 m/s. The tidal range at the landward end of the channel (L=60 km) is larger than that at the mouth (amplification).

Reducing the water depth to h=5 m (case 3) leads to a slight reduction of the tidal range over sections 0–40 km according to the numerical model (see Fig. 14). However, the numerical model results show that the tidal range is slightly amplified in the landward section of the channel (x=40–60 km) due to reflection. The analytical model can represent the reflection effects at the end of the channel reasonably well, but the computed tidal range in sections 25–55 km is much too small. Neglecting the reflection effect, the computed tidal range in the landward section based on the analytical model is much too small.

Figures 15 and 16 show the computed tidal range values along the long channel (L=180 km) for cases 5 and 6 with a converging channel over the entire length of the channel based on the DELFT2DH model and the analytical linearized model. The analytical model results without reflection for case 5 are in good agreement with the numerical model results, except in the landward end section of the channel (140–180 km). The analytical model with reflection for case 5 yields values which are substantially too small in the middle part of the channel. The effect of the reflected wave is too strong at the landward end of the channel. The analytical model yields values for case 6 which are much too small when the friction coefficient is based on the peak velocity at the mouth. The results for case 6 can be improved by using a smaller (channel averaged) characteristic peak velocity (see Fig. 16).

7 Nonlinear effects and tidal asymmetry

The offshore astronomical tide is composed of various constituents. The most important constituent is the semidiurnal M_2 component. The first harmonic of this constituent is M_4. Generally, the M_4 component is small offshore (amplitudes of about 0.1–0.2 m), but may increase within estuaries due to bottom friction and channel geometry (see Speer and Aubrey 1985). The M_2 component and its first harmonic M_4 dominates the nonlinear processes within estuaries. Nonlinear interaction between other constituents is also possible in shallow estuaries. Analysis of field

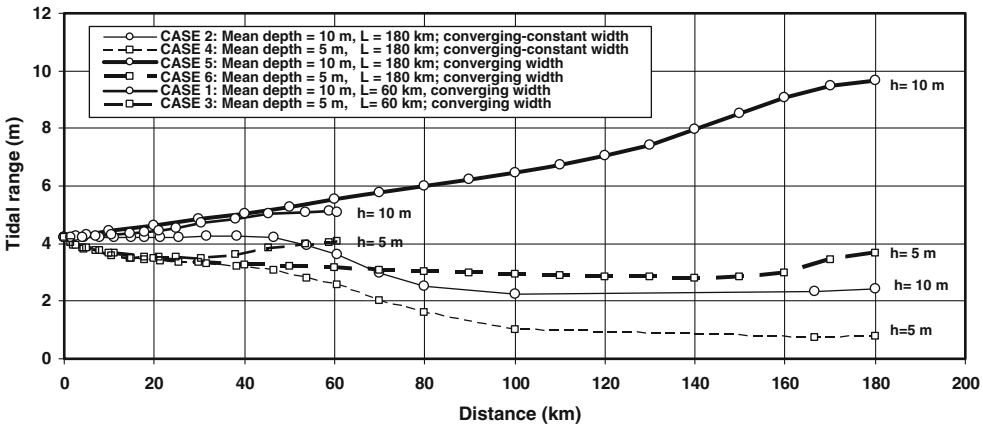

Fig. 13 Tidal range values for converging channel cases 1–6 based on numerical model DELFT2DH

Author's personal copy

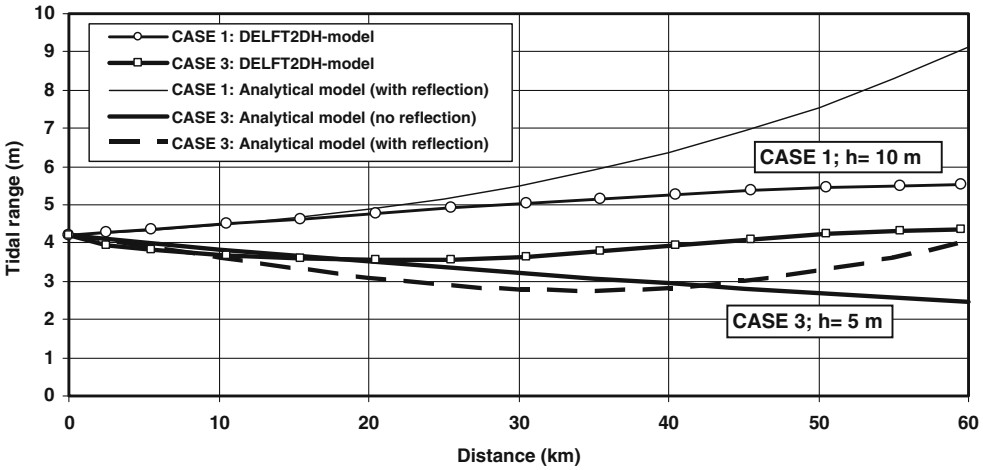

Fig. 14 Computed tidal ranges for converging channel cases 1 and 3 (L=60 km, h=10 and 5 m) based on DELFT2DH model and analytical model

observations has shown that interaction of M_2 and its first harmonic M_4 explains the most important features of tidal asymmetries.

The analytical solutions of the equations of continuity and momentum presented above do not express the nonlinear effects, as they are based on linear equations. All nonlinear terms ($\overline{u}\partial\overline{u}/\partial x$; $\partial(\eta\overline{u})/\partial x$ and u^2) have been neglected or linearized. Thus, the wave speed is constant and the peak flood and ebb velocities are equal (no asymmetry).

The generation of higher harmonics can be explained by the shallow water equations (Parker 1991). The wave speed without friction is $c=(gh)^{0.5}$ which is about constant if the wave height is small compared to the water depth ($\eta<<h$). In shallow water where η is not small compared to the depth, the wave crest will travel faster than the wave trough. The resulting wave profile will be distorted from a perfect sinusoidal wave profile giving a faster rise to HW and a slower fall to LW; HW will occur earlier and LW will occur later.

When η is not small compared to h, the velocity $\overline{u}$ cannot be neglected with respect to the wave speed c (Lamb 1963, 1966), so the wave speed at the crest is actually $c+\overline{u}$ and at the trough $c-\overline{u}$, which also results in wave asymmetry. This is the effect of the inertial term in the momentum equation $\overline{u}\partial\overline{u}/\partial x$ (which has been neglected in the analytical solutions). The importance of the inertial term is reduced by reflection making the wave closer to a standing wave, by friction and by the decrease of the width.

Nonlinear friction ($\overline{u}^2$) will also lead to distortion of the wave profile. The frictional loss per unit volume of fluid is smaller for greater depths and larger for smaller depths, so the crest will travel faster than the trough. Distortion of the wave profile (due to differences in bottom friction during flood and ebb) may also lead to a small, but gradual increase of the mean sea level at the end of the basin (mean sea level slope). For example, at the end of the Western Scheldt Estuary (The Netherlands), the mean water level is about 0.15 m higher than that at the mouth (Pieters 2002).

Other effects causing nonlinearity are: river flow and tidal flats. The river flow through the convective acceleration slows down the incident wave and speeds up the reflected wave. Tidal flats adjacent to the main channel lead to a loss of momentum on the rising tide when water pours

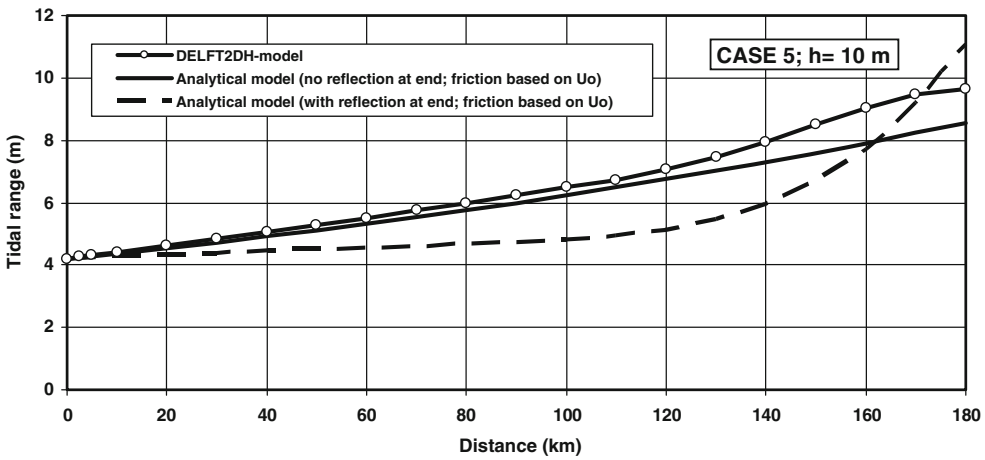

Fig. 15 Computed tidal ranges for converging channel case 5 (L=180 km, h=10 m) based on DELFT2DH model and analytical model

Author's personal copy

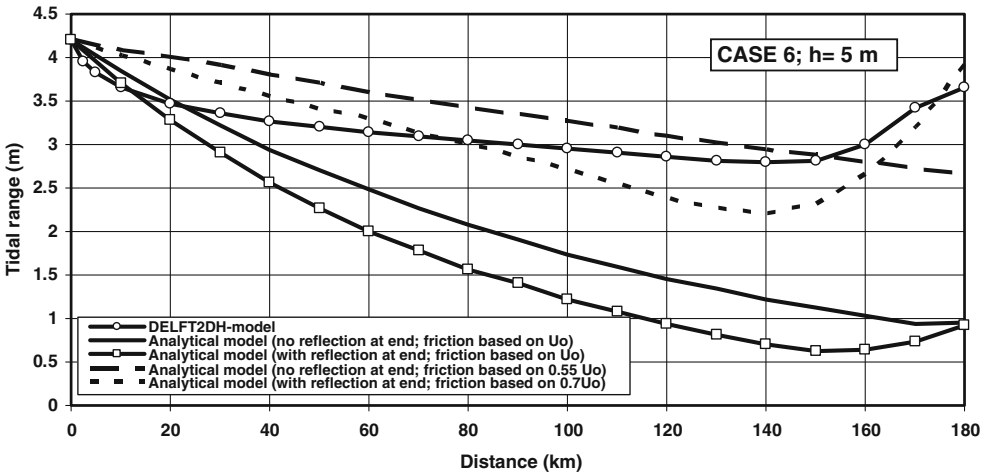

Fig. 16 Computed tidal ranges for converging channel case 6 (L=180 km, h=5 m) based on DELFT2DH model and Analytical model

out over the flats and also on the falling tide when almost zero-momentum water returns to the main channel where it will be accelerated (Jay 1991).

These nonlinear effects are fully taken into account by numerical models. Figures 17 and 18 show the HW and LW levels along the channel for cases 3 and 6 (small depth of h=5 m) based on the numerical model DELFT2DH and the analytical linearized model with reflection. These nonlinear effects are especially manifested in the shallow depth channels. The mean water level increases by about 0.3 m. The HW rise is much larger than the LW fall with respect to the mean water level (tidal asymmetry). The analytical model does not include the nonlinear effects resulting in a symmetrical solution with respect to MSL. Differences between both models are up to 1 m, particularly for HW.

8 Summary and conclusions

In this paper, new and old analytical models based on the energy flux and momentum equations have been presented to describe the tidal range for converging estuary channels. The energy-based approach allows the inclusion of nonlinear (quadratic) bottom friction. The analytical solution of the momentum equation is only valid for linear bottom friction. The linearized analytical solution of the momentum equation is presented for M_2 tidal waves with and without reflection in strongly convergent (funnel type) channels. The analytical solutions are compared with the results of numerical solutions and with measured data of the Western Scheldt Estuary in the Netherlands, the Hooghly Estuary in India, and the Delaware estuary in the USA. The analytical solutions show surprisingly good agreement with measured tidal ranges in these large-scale tidal systems. The analytical model also produces rather good results of the tidal range for the very large-scale Yangtze Estuary (Van Rijn 2011). The linearized analytical model is most accurate in the seaward part of the estuary where the width is large and the depth is almost constant and the river discharge is very small compared to the tidal discharge. Convergence of the width is found to be dominant in long and deep converging channels resulting in an amplified tidal range (L_b/h_o<4,500), whereas bottom friction is generally dominant in shallow converging channels resulting in a damped tidal range (L_b/h_o>4,500). Reflection against the landward end of a closed channel is important in the most landward

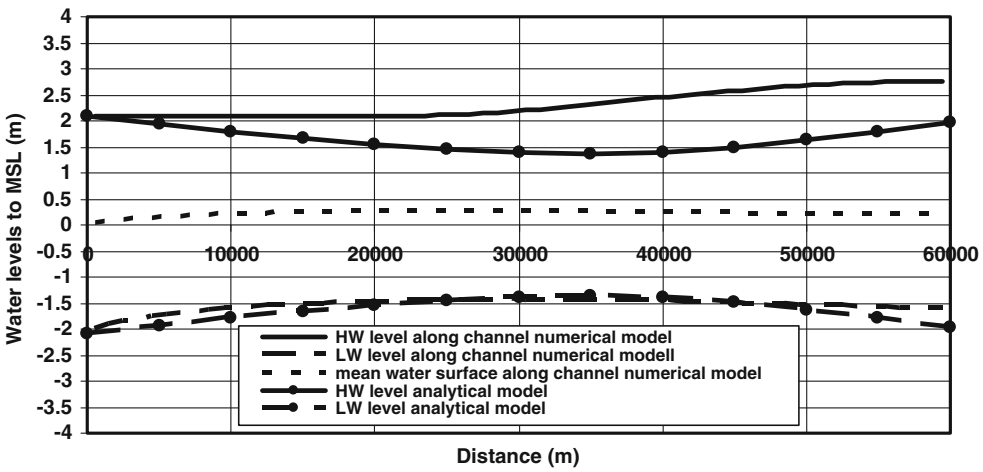

Fig. 17 Computed HW, LW, and mean surface level for converging channel. Case 3 (L=60 km, h=5 m) based on DELFT2DH model and analytical model

Author's personal copy

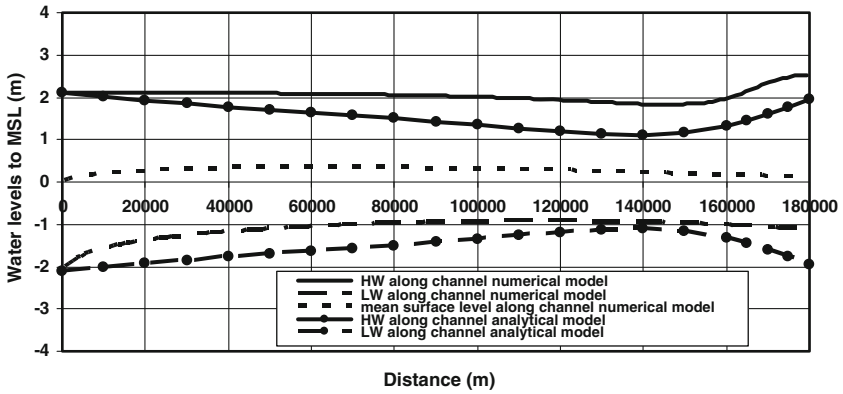

Fig. 18 Computed HW, LW, and mean surface level for converging channel. Case 6 (L=180 km, h=5 m) based on DELFT2DH model and analytical model

section with a length of about 1/3 of the total channel length. In strongly convergent channels with a single forward-propagating tidal wave there is a phase lead of the horizontal and vertical tide close to 90°, mimicking a standing wave system (apparent standing wave).

The analytical models offer simple and powerful tools for tidal analysis of amplified and damped tidal wave propagation in prismatic and converging estuaries. The simplicity and transparency of the analytical methods makes them very suitable for a quick scan of the most important tidal parameters when the effects of human interferences have to be evaluated such as the effects of dredging (channel deepening) and changes in water storage. It is also very suitable for combination with simple salt intrusion models (part II). The spreadsheet model (tidalmotion.xls) used by the author is freely available by email.

The results show that the analytical models can be used to obtain information of the basic trends of the solutions, but these models cannot deal very well with reflection in the most landward section of a converging channel with large depths (cases 1 and 5; h=10 m). The analytical models also are not very accurate in predicting the precise HW and LW levels, as nonlinear effects are not taken into account. Furthermore, linear friction is not very accurate for long tidal channels. This can be partly overcome by schematizing the channel into smaller subsections and applying the analytical model to each subsection. However, this latter approach is laborious and offers no real advantage with respect to numerical models, which also contain the nonlinear terms (so more physics). One-dimensional numerical models including all nonlinear terms can be setup easily and quickly, but do not give immediate insight into the most important processes involved. Many sensitivity computations are required to identify the dominant parameters. Analytical models offer the advantage of rapid identification of these dominant parameters and processes. Using analytical models, the parameter range can be narrowed down substantially so that the minimum number of numerical model runs need to be made.

Acknowledgments J. Dronkers of Deltares is gratefully acknowledged for his suggestions and checks improving the manuscript. Also, PK Tonnon of Deltares/Delft Hydraulics is gratefully acknowledged for performing and analyzing the DELFT2DH model runs.

Appendix I

The energy flux balance for depth-integrated tidal flow reads, as:

$$d\left(b\overline{F}\right)/\mathrm{dx} + b\,D_w = 0 \tag{1}$$

$$b\,\mathrm{d}\overline{\mathrm{F}}/\mathrm{dx} + \overline{\mathrm{F}}\mathrm{db}/\mathrm{dx} + b\,D_w = 0 \tag{2}$$

with $\overline{F}$=energy flux per unit width per unit time and D_w= energy dissipation per unit area and time due to bottom friction, b=width of estuary channel, x=horizontal coordinate (positive in landward direction, x=0=mouth). The unit of each term is kgm/s^3.

Since the work per unit time is defined as the product of force and velocity (=length per unit time), the instantaneous work done by the dynamic pressure force in a vertical section is:

$$F = \int_o^h P_d\,\overline{\mathrm{u}}\,\mathrm{dz} \tag{3}$$

The time-averaged (over the wave period) work done by the dynamic pressure force

$$\overline{F} = (1/T)\int_o^T\int_o^h (P_d\overline{u})dz\,dt \tag{4}$$

with, P_d=ρ gη=instantaneous pressure at height z above bed due to tidal water level variation, η=$\widehat{\eta}$ cos(ωt), $\overline{u}$=Q_r/(bh)+$\widehat{\overline{u}}$ cos(ωt + φ)=instantaneous tidal velocity at height z (assumed to be constant over the depth and equal to depth-averaged velocity), h_o=water depth to mean water surface level (h=h_o+η), b=width of estuary, Q_r=river

Author's personal copy

discharge, φ=phase lead of velocity maximum with respect to water level maximum.

Generally, $Q_r << Q_{\text{tide}}$. Thus:

$$\begin{aligned}
&\overline{F} = (1/T)\int_o^T\int_o^h (\rho\, g\, \eta\, \overline{u})dz\, dt = (\rho\, g\, h_o)(1/T)\int_o^T (\eta\, \overline{u})dt \\
&\overline{F} = [\rho\, g\, h_o\, Q_r/(bh_o)] + \left[\left(\rho\, g\, h_o\, \widehat{\eta}\, \widehat{\overline{u}}\right)(1/T)\int_o^T \cos(\omega t)\cos(\omega t+\varphi)dt\right] \\
&\overline{F} = [\rho\, g\, h_o\, Q_r/(bh_o)] + \left[\left(0.5\,\rho\, g\, h_o\, \widehat{\eta}\, \widehat{\overline{u}}\right)\cos(\varphi)\right] \\
&\overline{F} = [\rho\, g\, h_o Q_r/(bh_o)] + \left[\left(0.25\, g\, h_o\, H\, \widehat{\overline{u}}\right)\cos(\varphi)\right]
\end{aligned} \tag{5}$$

Using the characteristics of a progressive wave in deep water: $\widehat{\overline{u}}=(\widehat{\eta}/h_o)c_o=(0.5H/h_o)c_o$; $\varphi=0$; $\widehat{\eta}=0.5H$; $c_o=(gh_o)^{0.5}$ and assuming $Q_r=0$, it follows that:

$$\overline{F} = 0.125\,\rho\, g\, H^2 c_o = \overline{E}\, c_o \tag{6}$$

with $\overline{E}=0.125\ \rho g\, H^2$=energy of a wave per unit area, c_o= wave propagation velocity.

Thus, the energy flux per unit width of a progressive wave in deep water is equal to the energy of a wave per unit length of the wave and the wave propagation velocity (similar to the expression used in short wave theory).

The instantaneous energy dissipation per unit area and time due to work done by the bed shear stress is:

$$D_w = \tau_b\, \overline{u} = 0.125\,\rho\, f\, \overline{u}^2\, \overline{u} = 0.125\,\rho\, f\, \widehat{\overline{u}}^3\, \cos^3(\omega t) \tag{7}$$

with τ_b=bed shear stress=$0.125\ \rho f\, \overline{u}^2$, f=friction coefficient=$8\ g/C^2$, C=Chézy coefficient.

The time-averaged work done by the bed shear stress is:

$$\begin{aligned}
\overline{D}_w &= 0.125\rho\, f\, \widehat{\overline{u}}^3 (2/T)\int_o^{0.5T} \cos^3(\omega t)dt \\
&= \left(1/(6\pi)\right)\rho f\, \widehat{\overline{u}}^3 = \left(4/(3\pi)\right)\rho\left(g/C^2\right)\widehat{\overline{u}}^3
\end{aligned} \tag{8}$$

Using linearized friction according to the Lorentz (1922, 1926) method, the same result is obtained.

The width and depth of the estuary channel is represented as:

$$\begin{aligned}
&b = b_o \exp(-\beta x) = b_o \exp(-x/L_b) \text{ and thus} \\
&db/dx = -\beta\, b_o \exp(-\beta x) = -\beta\, b \\
&h = h_o \exp(-\gamma x) = h_o \exp(-x/L_h) \text{ and thus} \\
&dh/dx = -\gamma\, h_o \exp(-\gamma x) = -\gamma\, h
\end{aligned} \tag{9}$$

with b_o=width at entrance $x=0$, $\beta=1/L_b$=convergence coefficient, $\gamma=1/L_h$, L_b=convergence length scale for width, L_h= convergence length scale for depth. The length scale L_b is of the order of 10–50 km for most estuaries. The length scale L_h is much larger than L_b for most estuaries as the depth generally is fairly constant or very weakly decreasing in landward direction.

Assuming $Q_r \cong 0$ (no river discharge), the energy flux balance expression becomes (h_o=water depth to mean sea level at entrance=constant along x; $\widehat{\overline{u}}$=peak tidal velocity along estuary):

$$\begin{aligned}
&bd\overline{F}/dx + \overline{F}db/dx + b\, D_w = 0 \\
&bd\left[0.25\,\rho\, g\, h\, H\, \widehat{\overline{u}}\right)\cos\varphi\Big]/dx + \left[0.25\,\rho\, g\, h\, H\, \widehat{\overline{u}}\cos\varphi\right][-\beta\, b] + \left[\left(1/(6\pi)\right)\rho\, b f\, \widehat{\overline{u}}^3\right] = 0 \\
&0.25\, b\,\rho\, g\, \cos\varphi\, d\left[h\, H\, \widehat{\overline{u}}\right]/dx + \left[0.25\,\rho\, g\, h\, H\, \widehat{\overline{u}}\cos\varphi\right][-\beta\, b] + \left[\left(1/(6\pi)\right)\rho\, b f\widehat{\overline{u}}^3\right] = 0 \\
&\cos\varphi\, d\left[h\, H\, \widehat{\overline{u}}\right)\Big]/dx - \beta\, h\, H\, \widehat{\overline{u}}\cos\varphi + \left[\left(2/(3\pi g)\right)f\widehat{\overline{u}}^3\right] = 0 \\
&\cos(\varphi)\left[\widehat{\overline{u}}H\, dh/dx + \widehat{\overline{u}}h\, dH/dx + H\, h\, d\widehat{\overline{u}}/dx\right] - \beta\, h\, H\, \widehat{\overline{u}}\cos\varphi + \left[\left(2/(3\pi g)\right)f\widehat{\overline{u}}^3\right] = 0
\end{aligned} \tag{10}$$

Assuming, $d\,\widehat{\overline{u}}/\mathrm{d}x=\varepsilon\,\widehat{\overline{u}}$ and $\mathrm{d}H/\mathrm{d}x=\varepsilon H$ (with ε being a small parameter), it follows that: $\mathrm{d}\widehat{\overline{u}}/\mathrm{d}x=(\widehat{\overline{u}}/H)\ \mathrm{d}H/\mathrm{d}x$, resulting in:

$$\begin{aligned}
&\cos\varphi\left[\widehat{\overline{u}}H\ (-\gamma h) + 2\widehat{\overline{u}}\, h\, dH/dx\right] - \beta\, h\, H\, \widehat{\overline{u}}\cos\varphi + \left[\left(2/(3\pi g)\right)f\widehat{\overline{u}}^3\right] = 0 \\
&dH/dx = 0.5(\beta+\gamma)H - \frac{f\,\widehat{\overline{u}}^2}{3\pi\, g\, h\, \cos\varphi}
\end{aligned} \tag{11}$$

Using $\widehat{\overline{u}} = (0.5H/h_o)c\,\cos\varphi$ for a channel of constant depth h_o (see Table 1) and thus $\gamma=0$, it follows that:

$$dH/dx = 0.5\beta\, H - \frac{f\, H^2 c^2\, \cos\varphi}{12\pi\, g\, (h_o)^3} \tag{12}$$

with H=tidal range, $\beta=1/L_b$=converging length scale (e-folding length scale), h_o=depth (constant), $\widehat{\overline{u}}$=peak tidal velocity along channel, c=local wave speed, φ=phase difference between horizontal and vertical tide, $f=8\ g/C^2$= friction coefficient, C=Chézy coefficient, x=horizontal coordinate (positive in landward direction).

References

Davies LJ (1964) A morphogenic approach to the worlds' shorelines. Z Geomorphol 8:127–142

De Kramer J (2002) Water movement in Western Scheldt Estuary (in Dutch). Dep. of Physical Geography, Report ICG 02/6. University of Utrecht, Utrecht, The Netherlands

Author's personal copy

Dronkers JJ (1964) Tidal computations in rivers and coastal waters. North-Holland, New York, p 518
Dronkers J (2005) Dynamics of coastal systems. World Scientific, Hackensack, p 519
Dyer KR (1997) Estuaries: a physical introduction. Wiley and Sons, Aberdeen, UK
Friedrichs CT (1993) Hydrodynamics and morphodynamics of shallow tidal channels and intertidal effects. Ph. D. Thesis. Mass. Inst. of Technology, Woods Hole Oceanographic Inst. Woods Hole, Massachusetts, USA
Friedrichs CT, Aubrey DG (1994) Tidal propagation in strongly convergent channels. J Geophys Res 99(C2):3321–3336
Godin G (1988) Tides. Centro de Investigacion Cientificia y de Educacion Superior de Ensenada, Mexico
Green G (1837) On the motion of waves in a variable canal of small depth and width. Trans Cambridge Philos Soc 6:457–462
Harleman DRF (1966) Tidal dynamics in estuaries, part II: real estuaries. In: Ippen AT et al (eds) Estuary and coastline hydrodynamics. McGraw-Hill, New York
Hunt JN (1964) Tidal oscillations in estuaries. Geophys J R Astron Soc 8:440–455
Ippen A (1966) Tidal dynamics in estuaries, part I: estuaries of rectangular cross-section. In: Ippen AT et al (eds) Estuary and coastline hydrodynamics. McGraw-Hill, New York
Jay DA (1991) Greens's law revisited: tidal long-wave propagation in channels with strong topography. J Geophys Res 96(C11):20585–20598
Lamb H (1963, 1966) Hydrodynamics. Cambridge Press, Cambridge
Lanzoni S, Seminara G (1998) On tide propagation in convergent estuaries. J Phys Res 103:30793–30812
Le Blond PH (1978) On tidal propagation in shallow rivers. J Geoph Res 83:4717–4721
Le Floch JF (1961) Propagation de la marée dans l'estuaire de la Seine et en Seine-Maritieme. Centre de Recherches et d'études Océanographiques, Paris, France
Lorentz HA (1922) Including resistance in tidal flow equations (in Dutch). De Ingenieur, The Netherlands, p 695 (in Dutch)
Lorentz HA (1926) Report Commission Zuiderzee 1918–1926 (in Dutch). Den Haag, The Netherlands
McDowell DM, O'Connor BA (1977) Hydraulic behaviour of estuaries. MacMillan Press, London
Parker BB (1984) Frictional effects on the tidal dynamics of a shallow estuary. Doctoral Thesis. John Hopkins University, USA
Parker BB (1991) The relative importance of the various nonlinear mechanisms in a wide range of tidal interactions. In: Parker BB (ed) Tidal hydrodynamics. Wiley, New York, pp 237–268
Pieters T (2002) The tide in the Western Scheldt Estuary (in Dutch). Document BGW-0102. Consultancy tidal waters. Vlissingen: The Netherlands
Prandle D (2003a) Relationships between tidal dynamics and bathymetry in strongly convergent estuaries. J Phys Oceanogr 33:2738–2750
Prandle D (2003b) How tides and river flows determine estuarine bathymetries. Prog Oceanogr 61:1–26
Prandle D (2004) Salinity intrusion in partially mixed estuaries. Estuar Coast Shelf Sci 54:385–397
Prandle D (2009) Estuaries. Cambridge University Press, Cambridge
Prandle D, Rahman M (1980) Tidal response in estuaries. J Phys Oceanography 10:1552–1573
Savenije HHG (2005) Salinity and tides in alluvial estuaries. Elsevier, New York
Savenije HHG, Toffolon M, Haas J, Veling EJ (2008) Analytical description of tidal dynamics in convergent estuaries. J Geophys Res 113:C10025
Speer PE, Aubrey DG (1985) A study of non-linear tidal propagation in shallow inlet/estuarine systems, part II: theory. Estuarine, Coastal Shelf Science 21:207–224
Van Rijn L (1993, 2011) Principles of fluid flow and surface waves in rivers, estuaries, seas and oceans. Aqua Publications, The Netherlands, p 750, www.aquapublications.nl
Verspuy C (1985) Lecture notes: long waves (in Dutch). Delft University of Technology, Delft, The Netherlands